Title

Phosphorylation of HP1/Swi6 relieves competition with Suv39/Clr4 on nucleosomes and enables H3K9 trimethyl spreading.

Author

Kennedy, Dana Renae

Publication Date

2024

Peer reviewed|Thesis/dissertation

Phosphorylation of HP1/Swi6 relieves competition with Suv39/Clr4 on nucleosomes and enables H3K9 trimethyl spreading.

by
Dana Renae Kennedy

DISSERTATION
Submitted in partial satisfaction of the requirements for degree of
DOCTOR OF PHILOSOPHY

in

Biochemistry and Molecular Biology

in the

GRADUATE DIVISION
of the
UNIVERSITY OF CALIFORNIA, SAN FRANCISCO

Approved:

Signed by:
John Gross
72366174074B4F4...

John Gross
Chair

DocuSigned by:
Bassem Al-Sady
DocuSigned by:
EE2E6D32EE3043B...

Bassem Al-Sady

Geeta Narlikar

Committee Members

ACKNOWLEDGEMENTS

My relationships with people are what propels me forward. I would not have been able to move through this PhD without the love and support from my friends and family.

I first want to acknowledge and thank my mom and dad, Lorrinda and Steve Kennedy. My mom is an avid reader, and I have fond memories of us spending hours in the library and bookstores growing up, as well as her reading the Berenstain Bears stories to me. My mom is the most selfless and kind person, and she has always been there for my brothers and me. My dad and I spent a lot of time together fishing, camping and woodworking in the garage. He taught me to measure twice and cut once, which was very applicable in graduate school when I needed to check my calculations twice and pipette once. My parents never pushed me to do anything I didn't want to do. They always supported me in anything I wanted to pursue, and I am so grateful to have them as my first teachers. Thank you for giving me the freedom to make choices for myself and thank you both for supporting me in all that I do. I love you.

To my brother, Joel "Joey" Kennedy, the artist. I think we texted just about every single day throughout graduate school. You have always been my biggest protector and cheer leader. We shared so much growing up, from our love of art, music, movies, being the biggest goof balls, and dreaming together. One of your best qualities is your sense of humor. No one laughs as hard as we do together. Thank you for never letting me forget who I am and where I come from. I love you. I will also mention our older brother, Kyle. Though you are not present in my life, I acknowledge that you impacted who I am today, and I do think you've supported my educational pursuits from afar.

I next want to thank individuals from my undergraduate institution, San Francisco State University. I first want to thank Phil Klasky, my first teacher on pedagogy, the art of teaching. In my first semester at SFSU I took Phil's American Indian Studies course, AIS 235 American Indians: Image and Issues in the Mass Media. At the end of the semester, Phil asked me to be his teaching assistant, a role I held for three years. During that time, I not only observed his

teaching methods but was also given the opportunity to teach and develop lectures for his classes. Phil taught me the importance of respecting and uplifting people from diverse cultures, backgrounds, and experiences, both inside and outside the classroom. This perspective now shapes all my interactions in life. Thank you, Phil. To the Student Enrichment and Opportunity office and Dr. Frank Bayliss— thank you for giving me the opportunity to be a NIH-MARC scholar and for giving baby scientist Dana the resources to progress towards a PhD program. To Dr. Raymond Esquerra— thank you for giving me my first research opportunity. Your lab was a safe space for me to grow as a scientist and you truly believed in me. The Esquerra lab— you all felt like family. Shout out to Heme Team: Bushra and Adriana who were my first mentors in the lab. You both are so brilliant, and I am grateful to have two amazing friends with whom I also had the opportunity to work closely and collaborate with. To Sita, my first mentee, you were and still are a bright light in my life, and I am so proud of you.

To my SFSU besties: Juliana Nzongo, Angela Amorello, Amy Wong, Scott Campit, and Chichi Okorie— I am so glad we found each other. Somehow, we all came together in undergrad and developed this inseparable, wholesome squad. You all are like my sisters, including Scott, in the best possible way. Thankfully we had zoom during the pandemic to continue growing our bond. We can have the deepest conversations that are filled with comedic relief. And we supported one another as we left SFSU and navigated grad school together. I am so proud of each of you and your accomplishments. I love you and thank you.

As an undergraduate I had the opportunity to do a Summer Research Training Program at UCSF in Dr. Dorit Ron's neuroscience lab, and I want to thank her as well as my direct mentors, Sophie Laguesse and Aude Bouagnon. Dr. Ron— thank you for giving baby scientist Dana an opportunity to learn neuroscience and for supporting me in my graduate school endeavors. To Sophie— I was, and still am, awestruck by your scientific rigor. To Aude, PhD soon to be MD— I am so grateful you were paired with me as my summer mentor. You are one of the most empathetic and brilliant people I have met, and I know you will make the best doctor

a patient could ask for. I also want to thank my roommate that summer, Ale Castruita. Ale— I truly thank whatever UCSF algorithm matched us, because you will be my friend for life. You are one of the funniest people I know, and I am so proud of the scientist you have become. I love you.

When I interviewed at UCSF, it was Muryam Gourdet who convinced me to come here and told me this community needed me. And here we are 7 years later. Thank you for being a true friend Muryam.

To the Al-Sady lab. My thesis advisor, Dr. Bassem Al-Sady— thank you for giving me the space to develop this project and trusting where I was able to take it while learning to be a scientist. Thank you for stepping in not only as my PI but as a scientific peer. I learned a lot from you these past 6 years. Henry Ng— you were and always will be my lab hermano. You gave me the gift of your time, not only helping me develop my experiments but, also pushing me to be the best version of myself. I wouldn't be the person I am inside and outside of science without you. I really don't think there is anything that you cannot do. You're a truly amazing scientist, cook, crafter, and the list goes on. I love you. Eric Simental— you inspired me to be the best scientist I could be. You made me feel seen and never ceased a moment to gas me up. Thank you for always offering your help before I needed to ask. I am so proud of the scientist you became during grad school, excited to see where your post doc takes you, and I look forward to our friendship evolving outside of this experience. Lena Kallweit— life with you is fun. Period. I cherished our adventures together, from roller skating in the parking lot after lab to our coffee dates; I remember us always laughing whatever we were getting into. I am super proud of you for finishing up your PhD and can't wait to see what you do next, Leña! Nick Sanchez— you were patient with me when I had a question, or when I wanted you to watch me inject my protein on the FPLC for the 6th time because I was afraid of breaking it. I also remember us laughing a lot. Navigating the first few years of graduate school often felt like the 5th dimension, so thank you for grounding me. Lucy Brennan and Madeline Keenen— there were many points along the

way where each of you took time to help me think through this project and provide feedback. I have learned so much from both about how to be a scientist. You both are my scientist role-models and dear friends. Thank you so much for your love and support.

Past and present members of the Al-Sady lab: R.A. Greenstein, Kif Lim, Can Goksal, Farzad Yousefi, Eric Martin, Ahmed Amine Mergani, Sophia Jia, Nathan Ho, Perla Abi Kheirs, Ann Raja-Somu, Bulut Hamali, Liv Jensen, Cal Clemmer, Daniel Darling, and Agnis Mazumder. I felt like I was at the center of a revolving door and all these amazing individuals were starting in the lab; then, before I knew it, they were transitioning on to their next step in life. Our lab is a launching pad for all of us. No one understands this journey like you all do. I am thankful for each one of you and stoked for all your futures.

This project would not have come this far without my qualifying exam and thesis committee members: Barbara Panning, Abby Buchwalter, Geeta Narlikar, and John Gross. Barbara— thank you for all your support during my first year and as my qualifying exam chair. We had many discussions about this project in its infancy, and I hope it makes you proud that I was able to bring it to life. Thank you so much for the care you've given to me in training me to be a scientist. Abby— thank you for your dedication to seeing me through quals and for your thoughtful questions. And thank you for supporting my ChIP-seq endeavors. Geeta— your scientific rigor is a level I aspire to be, and you make science fun. Thank you for investing time into me as a budding scientist and for all our conversations pushing this project forward. John— each time we met you made me feel like a scientific peer and it gave me a lot of confidence in myself that I could drive my project forward. You not only saw me as a scientist but a person. Thank you for your dedication as my chair.

My experiments would not have been possible without the coordination and support of the Hooper Foundation Administration: Bernarda Lopez, Ernesto Valencia, Daryll Gempis, and Ethel Enoex-Godonoo. Grad school would not have been the same without seeing each of you every day. Thank you for making my days in the Hooper brighter.

I want to thank the Tetrad Program Administration: Toni Hurley, Danny Dam, Billy Luh, and Veena Mohan. Toni— you really hold it down. Thank you so much for all you do for Tetrad and the students, for always helping me out when I had a question. I always enjoyed our catchups in your office. Also, thank you to Danny, Billy and Veena for supporting the students and coordinating events.

Dr. D'Anne Duncan started as Assistant Dean for Diversity and Learner Success in the Graduate Division the same year I started grad school, and I am so grateful our journeys aligned. D'Anne— you always made me feel seen and heard, and you were always looking out for me both personally and professionally. You inspire me to be the best educator, scientist, and person. Thank you for the support and mentorship throughout the last 7 years.

To the Society for the Advancement of Chicanos/Hispanics and Native Americans in Science— Dina Buitrago Silva, Ramiro Patino, Veronica Escalante, Donovan Trinidad, Elise Muñoz, Harold Marin, Jose Liboy, Jocy Lopez, Evelyn Hernandez, Karina Perlaza, our advisor Dr. David Booth, and all the members. Some of my best memories in graduate school are working with all of you to uplift our community here at UCSF and beyond. You each are driven to leave this world better than you received it. We worked really hard, but also had a lot of fun, and I hope after grad school we still go out and tear up the dance floor together.

Somehow, the stars aligned and the Tetrad entering class of 2017 was a group of incredible individuals, many of whom I developed lifelong friendships with. To Gabi Canales— the Romy to my Michelle, you are the sister I never had growing up. From thrifting together, living together, crying in public together. I am so grateful to be in your orbit. You have stuck by my side since we started grad school. You have been my rock through this experience, especially the final months. We go from the most serious, healing conversations, to literally playing like children. The way you have advocated for yourself and your personal growth through this experience inspires me. Thank you for reminding me to enjoy life, to play, to create. You'll be in my life for eternity. I love you. Elise Muñoz— There is so much to say and so little

time. Elise, you think about things so deeply and I learn from you every day. No one understands me like you do. You're my best friend, my soul mate, my rock. You literally excel in everything you put your heart into. I am so proud of you for taking huge bites out of life, especially in you new chapter in San Diego. Thank you for loving me. I will cherish you forever. To Ady Steinbach and Francesca Del Frate, two of the most creative people I have ever come across. Ady— thank you for being the best Hooper buddy. I am inspired by all that you do, in and out of science, and I am excited to see what is next for you. I often leave our conversations feeling seen and validated, and you highlight things that I have yet to see in myself. Thank you, bb. Fran— First year of graduate school we were the two Sunset commuters, taking the grey shuttle to the N line, and I look back fondly on that time together. Also, thank you so much for sitting with me over coffee and walking me through how to prepare the library for ChIP-seq. I followed my notes from our meeting, and everything worked the first time; we know that never happens in science. Science is more fun when you get to do it with friends like you. I really appreciate you and the perspectives you give on life. Thank you. Varun Bhadkamkar— your superpower is storytelling and asking the best, deepest questions. Thank you for reminding me of how loved I am and protecting my heart. I've said it over and over, but you are the brightest sparkle I've ever encountered. You light up the room. I love you very much. To our adopted classmates— Luke Strauskulage and Donovan Trinidad. Luke— I live for your one-liners and the belly laughs. You have such a balanced perspective on just about any topic. Thank you for keeping me grounded during this experience. I look forward to more beer and hangs with you. Don— The kindest and funniest person with the best dance moves. You have mastered the art of conversation and communicating. I think it's a skill you've honed because you're a great listener. When we talk you ask me questions that I find incredibly valuable and helpful to further process what I'm thinking or feeling. I always leave our hangs feeling like my cup is filled; thank you for being such a good friend to me.

I also want to mention grad school classmates and friends that made my life brighter: Chris Carlson, Hanako Gallager, Danny Conrad, Natalie Whitis, Amanda Chung, Ben Herken, Manny Richter, Gabby Estevam, Victor Lam, Janine Sengstack, Joy Li, Haley Gause, Katie Augspurger, Lili Kim, Liz Bond, CJ San Felipe, Luis Santiago, Sydney Williams, Hayden Sunders, Tom Moss, Josh Stein, Kelly Pan, Marisol, and literally anyone I potentially forgot. I tired my best to make a comprehensive list!

To my longest friendships from high school: Megan Azevedo, Vanessa Cortez, and Tyler Menjivar. We grew up together, even in adulthood, and I thank each of you for sticking by my side. Megan, my twinnie— you are the most loving and giving person with the biggest heart. You never forget to remind me how loved I am. Vanessa— you are brilliant in many ways. You give me the best life advice and keep my head on my shoulders. Tyler— every time we hang out it feels like an adventure. I admire how much you take risks on yourself and go for what you want. Thank you for endless laughs and life advice.

Lastly, I want to thank myself, especially my younger self, who all of this was really for. We did it, baby.

CONTRIBUTIONS

Chapter 2 of this dissertation is from a manuscript submitted for publication with the following authors: Dana Kennedy, Joël Lemiere, Catherine Tan, Eric Simental, Julian Braxton, Robert A. Maxwell, and Bassem Al-Sady.

Phosphorylation of HP1/Swi6 relieves competition with Suv39/Clr4 on nucleosomes and enables H3K9 trimethyl spreading.

Dana Kennedy

ABSTRACT

Heterochromatin formation in *Schizosaccharomyces pombe* requires the spreading of histone 3 (H3) Lysine 9 (K9) methylation (me) from nucleation centers by the H3K9 methylase, Suv39/Clr4, and the reader protein, HP1/Swi6. To accomplish this, Suv39/Clr4 and HP1/Swi6 have to associate with nucleosomes both nonspecifically, binding DNA and octamer surfaces and specifically, via recognition of methylated H3K9 by their respective chromodomains. However, how both proteins avoid competition for the same nucleosomes in this process is unclear. Here, we show that phosphorylation tunes the nucleosome affinity of HP1/Swi6 such that it preferentially partitions onto Suv39/Clr4's trimethyl product rather than its unmethylated substrates. Preferential partitioning enables efficient conversion from di-to trimethylation on nucleosomes *in vitro* and H3K9me3 spreading *in vivo*. Together, our data suggests that phosphorylation of HP1/Swi6 creates a regime that relieves competition with the "read-write" mechanism of Suv39/Clr4 for productive heterochromatin spreading.

TABLE OF CONTENTS

LIST OF FIGURES

LIST OF TABLES

1. Introduction

The basic unit of eukaryotic life is the cell, which carries all the genetic information needed to support life. Stem cells have the potential to differentiate into various cell types, forming tissues that support the function of organs. These organs, in turn, provide specialized functions that sustain an organism, from a hummingbird to a human.

Each cell contains the exact same genetic information, DNA, comprising chromosomes in the nucleus. DNA must be regulated and organized so that the cell can process it, thereby determining its identity and function. A key aspect of this organization involves packaging DNA into nucleosomes, in which 147 base pairs (bp) of DNA are wrapped around the histone octamer consisting of two H2A/H2B dimers and one H3/H4 tetramer. The nucleosome is the fundamental structural unit of chromatin, playing a critical role in the higher-order organization of DNA in the nucleus.

One of the earliest insights into how chromatin organization influences gene expression was observed by Dr. Emil Heitz in 1928. He developed a cytological staining technique that allowed him to visualize individual nuclei and distinguish two different regions of the genome, which he termed “euchromatin” and “heterochromatin”[74]. Euchromatin was the lightly stained region of the genome that he hypothesized was transcriptionally active, meaning genes were accessible and turned on. However, heterochromatin was the darkly, densely stained regions of the genome, which Heitz proposed was a structure where genes were inaccessible to transcriptional machinery, and thus turned off. Heitz identified this pattern in over 100 plant species and several fly species. His prediction was validated by a series of cytological, biochemistry, and genetics experiments in various model organisms, including *Drosophila melanogaster*, which confirmed the repressive nature of heterochromatin[3]. These foundational discoveries, among others in the early 20th century, opened the field of chromatin biology and epigenetics.

Today, after almost a century of scientific discoveries in chromatin biology, we understand that two key classes of proteins drive heterochromatin formation. One is termed a “writer”, or a

histone methyltransferase, which deposits methyl marks on lysine 9 residues of Histone 3 (H3K9). H3K9 methylation is the repressive mark that turns genes off. After H3K9 methylation is deposited, a “reader” protein, Heterochromatin Protein 1 (HP1), engages the H3K9 methyl mark and spreads along chromatin, creating a platform for other heterochromatin factors to bind and further define the gene repressive macrostructure[1].

There are numerous model organisms to study heterochromatin and gene regulation. In this work, we used a type of yeast called *Schizosaccharomyces pombe* (*S. pombe*). *S. pombe* is an ideal organism to study heterochromatin because the size of its genome is a fraction of the human genome. *S. pombe* has 3 chromosomes made up of 14 million base pairs, whereas the human genome is made up 46 chromosomes and 3.2 billion base pairs. In human cells, heterochromatin formation involves six H3K9 methyl writers and three heterochromatin readers. However, *S. pombe* relies on a simpler system with only one H3K9 methyltransferase, Clr4, and one key reader, the HP1 homolog called Swi6, which facilitates heterochromatin spreading. After Clr4 deposits H3K9 di- and trimethylation (H3K9me2 and me3), Swi6 engages with the methyl mark, oligomerizes along the modified nucleosomes, and recruits additional proteins that promote and maintain the heterochromatin domain[1].

It was previously shown that Swi6 was post-translationally modified with phosphorylation at several serine residues[27]. Mutation of these serines to alanines disrupted transcriptional gene silencing. Yet, the mechanism by which phosphorylated Swi6 regulates heterochromatin spreading, and therefore gene silencing, remains unknown. Thus, in this study we asked three main questions: 1. How does phosphorylation of Swi6 regulate nucleation and/or spreading of heterochromatin *in vivo*? 2. How does phosphorylated Swi6 regulate oligomerization and binding to the nucleosome *in vitro*? And finally, addressing these questions led us to the third question: Does the Swi6 reader help the Clr4 writer modify nucleosomes?

2: Phosphorylation of HP1/Swi6 relieves competition with Suv39/Clr4 on nucleosomes and enables H3K9 trimethyl spreading.

2.1 Introduction

Heterochromatin is a gene-repressive nuclear structure conserved across eukaryotic genomes[1]. Heterochromatin assembly requires seeding at nucleation sites and lateral spreading over varying distances to define a silenced domain[2]. In one highly conserved heterochromatic system, the spreading process requires at least two components: First, a "writer" enzyme, a suppressor of variegation 3-9 methyltransferase homolog (Suv39, Clr4 in *S. pombe*), which deposits Histone 3 lysine 9 methylation (H3K9me)[3]. Spreading by this H3K9 methylation "writer" depends on a positive feedback relationship in which the "writer" also contains a specialized histone-methyl binding chromodomain (CD) that recognizes its own product, H3K9me[4,5]. Second, spreading then further requires a "reader" protein[3,6,7], Heterochromatin Protein 1 (HP1, Swi6 in *S. pombe*), that also recognizes H3K9me2/3 via a CD[8].

How do HP1 proteins execute their essential function in heterochromatin spreading? One manner in which they do so is by directly recruiting the Suv39 methyltransferase to propagate H3K9 methylation[9–11]. Second, HP1 proteins oligomerize on H3K9me-marked chromatin, which has been invoked as a mechanism that supports spreading[12]. HP1 oligomerization also underlies its ability to undergo Liquid-Liquid Phase Separation (LLPS) *in vitro* on its own or with chromatin[13–15], and condensate formation *in vivo*[13,14,16,17]. This condensate formation may promote spreading by providing a specialized nuclear environment that concentrates HP1 and its effectors[18] and/or excludes antagonists of heterochromatin[13]. The silencing of heterochromatin by HP1 may be coupled to spreading by oligomerization, which likely promotes chromatin compaction and blocks RNA polymerase access[19,20]. Silencing may also require oligomerization-independent mechanisms like HP1's ability to bind RNA transcripts and recruit RNA turnover machinery[21,22].

However, these proposed mechanisms for HP1's role in spreading do not contend with a central problem, which is that HP1 and Suv39/Clr4 directly compete for the same substrate on multiple levels. This competition can be specific, as HP1 and Suv39/Clr4 have CDs that recognize the H3K9me2/3 chromatin mark[12,23]. It is also non-specific, as both HP1 and Suv39/Clr4 bind DNA and histone octamer surfaces of the nucleosome substrate[5,17,23–26]. How can HP1 promote H3K9 methylation spreading by Suv39/Clr4 but not get in its way? One explanation for managing the specific competition is an observed difference in methylation state preference. Clr4, for example, is more selective for the terminal trimethylated (H3K9me3) state than Swi6 or the other HP1 paralog in *S. pombe,* Chp2[23]. However, how the significant H3K9me3- independent nucleosome affinity of Clr4 and Swi6 is coordinated to avoid competition is not clear.

One possible way to regulate competition in spreading is through post-translational modifications of HP1. For example, HP1a, HP1α, and Swi6 are phosphorylated by CKII protein kinases[27–29]. Phosphorylation of HP1 across species has been shown to regulate multiple of its biochemical activities including LLPS[13], specificity for H3K9me[13,30], and affinity for nucleic acids[30]. In *S. pombe*, several Swi6 *in vivo* phosphorylation sites have been documented in the N-terminal extension (NTE), the CD, and the hinge domain[27], which, when mutated, disrupt transcriptional gene silencing[27]. Whether Swi6 phosphorylation regulates silencing through nucleation, spreading, or downstream processes is still unknown. It is also unclear how phosphorylation biochemically impacts Swi6's engagement with chromatin or Suv39/Clr4.

In this study, we focused on previously identified Swi6 phosphorylation target sites and found that two sites in particular, S18 and S24, are required for the spreading, but not nucleation, of heterochromatin[27]. Spreading defects in Swi6 S18/24A mutants arise due to a disruption of H3K9me3 spreading, but not H3K9me2 spreading. We show biochemically that the primary role of phosphorylation is to lower Swi6's overall chromatin affinity. This lowered affinity preferentially partitions Swi6 onto H3K9me3 nucleosomes, rather than unmethylated

nucleosomes, *in vitro* and into heterochromatin foci, rather than the nucleoplasm, *in vivo.* It may appear counter-intuitive that lowered affinity should have this effect. However, since phosphorylation also increases Swi6's propensity to oligomerize, this ultimately reduces the Swi6 pool available to bind unmethylated sites. We propose that phosphorylation of Swi6 frees up Clr4's substrates for efficient trimethylation, and thus, spreading.

2.2 Results

Serines 18 and 24 are necessary for heterochromatin spreading but not nucleation.

Previously, several phosphoserines in Swi6 have been shown to play a role in heterochromatin gene silencing[27] (**Figure 2.1A**). To address whether the phosphorylation targets play a role in nucleation and/or spreading of heterochromatin, we used our mating type locus (MAT) heterochromatin spreading sensor (HSS[31,32]) (**Figure 2.1B**). The HSS allows us to separate nucleation and spreading events at single-cell resolution via three separate transcriptional reporters: "green" at nucleation sites, "orange" at spreading sites, and "red" in a euchromatic site to control cell-to-cell noise[31,32]. Specifically, we used a MAT locus HSS with only the *cenH* nucleator intact (MAT *ΔREIII* HSS[32]), which enables us to isolate spreading from one nucleator.

To query *swi6* serine-to-alanine (S-A) mutants in this background, we first replaced the *swi6* open reading frame with the *ura4* gene (*swi6::ura4*). Using homologous recombination, we then replaced the *ura4* cassette with either wild-type or S-A mutant *swi6* open reading frames followed by a kanamycin resistance marker (**Figure 2.1B**). We based our S-A mutations on the phosphoserines previously identified in *Shimada et al.,* which include S18, S24, S46, and S52 in the NTE, S117 in the CD, and S192, S212, and S220 in the hinge (**Figure 2.1A**). Here, we constructed the following S-A mutants: S18A and S24A (*swi6*$^{S18/24A}$); S46A and S52A (*swi6*$^{S46/52A}$); S46A, S52A, S117A, S192A, S212A, and S220A, (*swi6*$^{S46/52/117-220A}$, "S18/S24 available"); and S18A, S24A, S117A, S192A, S212A, and S220A (*swi6*$^{S18/24/117-220A}$, "S46/S52 available"). These mutants are expressed at similar levels compared to wild-type as assessed by western blot, using a polyclonal anti-Swi6 antibody (**Figure 2.1C,** further validated by cytometry in **Figure 2.8C**).

When analyzed by flow cytometry, *Δswi6* cells exhibit a silencing defect in which both the nucleation ("green" on) and spreading ("orange" on) reporters are expressed (**Figure 2.1D**). Conversely, wild-type *swi6* cells show robust silencing of both reporters (**Figure 2.1E**). Mutating

only S46 and S52 to alanines (*swi6*$^{S46/52A}$) largely phenocopies wild-type *swi6* (**Figure 2.1F**). In contrast, mutation of serines at 18 and 24 (*swi6*$^{S18/24A}$) resulted in loss of spreading ("orange" on), while maintaining proper nucleation ("green" off) (**Figure 2.1G, Figure 2.2A-C**). Restoring S18 and S24, while mutating the other 6 serines to alanines (*swi6*$^{S46/52/117\text{-}220A}$) recovers nucleation and spreading to an almost similar degree as wild-type, though with a modest silencing loss at "orange" (**Figure 2.1H, 2.2D-F**). Thus, S18 and S24 play a dominant role in regulating spreading, while other serines make a minor contribution. However, when only S46 and S52 are available (*swi6*$^{S18/24/117\text{-}220A}$), cells not only exhibit a loss of spreading ("orange" on) but also a moderate loss of silencing at the nucleator ("green" shifted towards on) (**Figure 2.1I**). Hence, serines in the CD and hinge make a further minor contribution to Swi6's overall silencing role, which is revealed only in the context of S18/24A. Overall, we interpret these results to indicate that NTE serines 18-52 contribute to regulating spreading, with S18/24 as major and 46/52 as minor contributors.

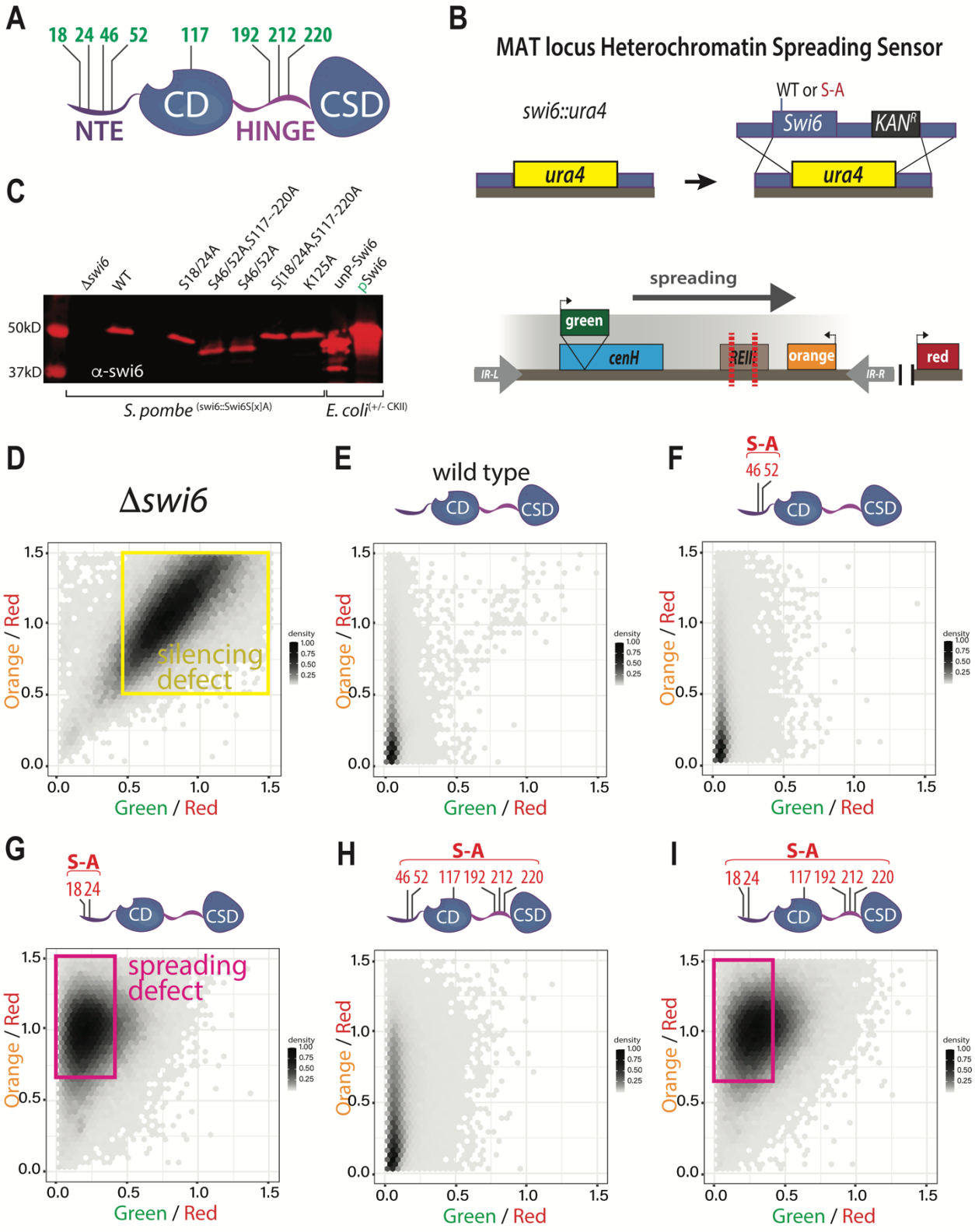

Figure 2.1 S18 and S24 in Swi6 are required for spreading, but not nucleation of heterochromatin silencing. A. Overview of the Swi6 protein domain architecture and
(Figure caption continued on the next page.)

(Figure caption continued from the previous page.)
previously identified[27] *in vivo* phosphorylation sites (green residue numbers). NTE: N-terminal extension; CD: chromodomain (H3K9me binding); HINGE: unstructured hinge region; CSD: chromo-shadow domain (dimerization and effector recruitment). **B.** Strategy for production of *swi6* S-A mutants in the MAT *ΔREIII* HSS reporter background. **C.** Swi6 levels are not affected by S-A mutations. Total extracts of *swi6* wild-type or indicated mutants were probed with an anti-Swi6 polyclonal antibody. *In vitro* purified Swi6 that was either phosphorylated (pSwi6) or not (unpSwi6) is run as size controls. **D.-I.** 2-D Density hexbin plots examining silencing at nucleation "green" and spreading "orange" reporter in *Δswi6,* wild-type, and indicated S-A mutants. The yellow box indicates a "green" and "orange" regime consistent with silencing loss, and the magenta box indicates a regime consistent with loss of spreading, but not nucleation.

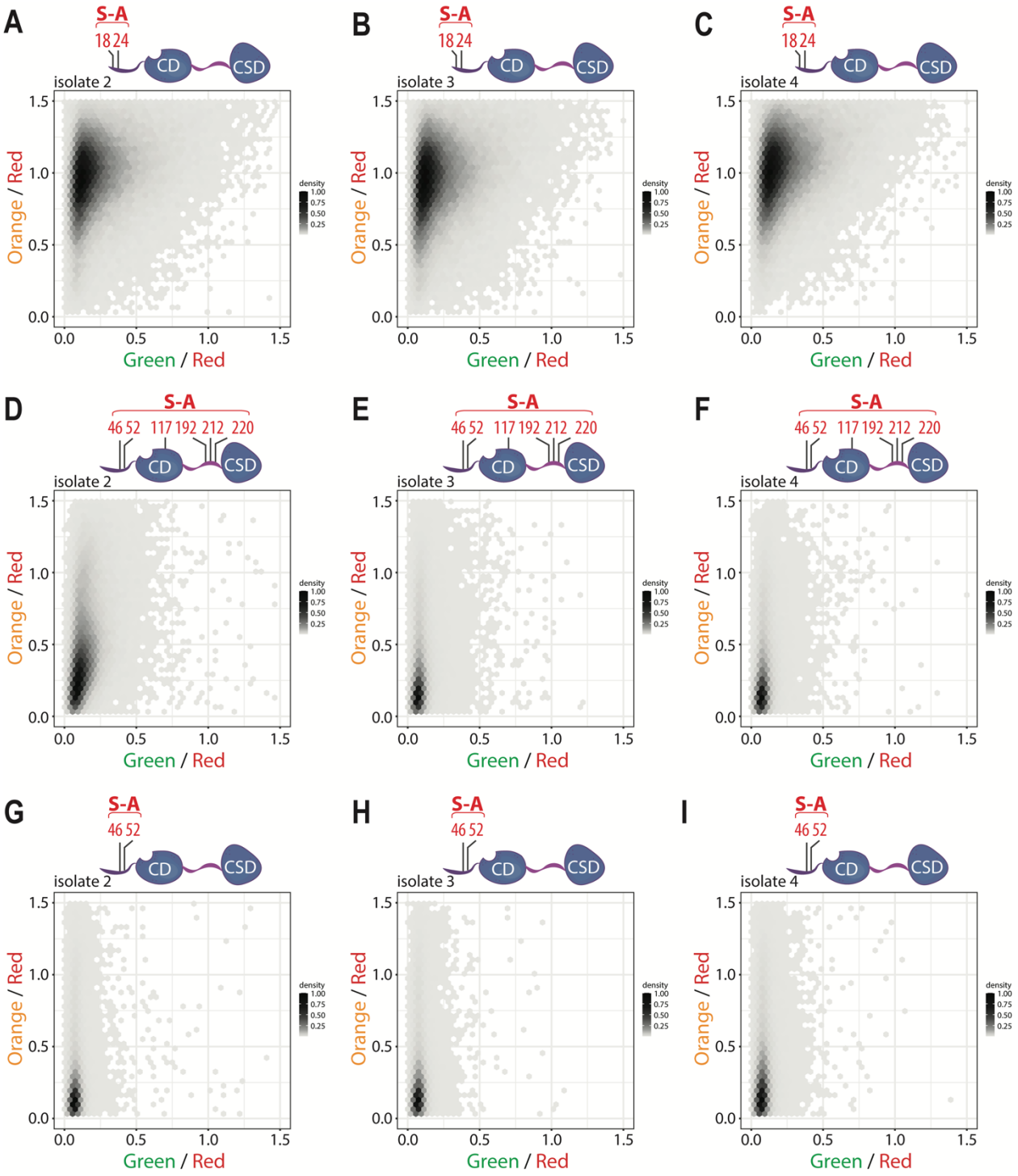

Figure 2.2 Additional isolates demonstrating that S18 and S24 in Swi6 are required for spreading, but not nucleation of heterochromatin silencing. 2-D Density hexbin plots examining silencing at nucleation "green" and spreading "orange" reporter in the MAT *ΔREIII* HSS for three additional isolates of **A.-C.** *swi6*$^{S18/24A}$ mutants, **C.-F.** *swi6*$^{S46/5/117-220A}$ ("S18/24 available"), and **G.-I.** *swi6*$^{S46/52A}$.

Serines 18 and 24 are required for the spreading of H3K9me3 but not H3K9me2.

We next asked how phosphorylation of S18 and S24 contributes to the propagation of heterochromatic histone marks. We used chromatin immunoprecipitation followed by sequencing (ChIP-seq) to address how levels of the heterochromatic marks, Histone 3 lysine 9 di- and trimethylation (H3K9me2/me3), are affected in the context of wild-type *swi6*, *swi6*$^{S18/24A}$, and *Δswi6* in the MAT *ΔREIII* HSS background containing the "green" and "orange" reporters (**Figure 2.3A**). Consistent with prior work, we define H3K9me2 as the heterochromatin structural mark[33] and H3K9me3 as the heterochromatin spreading and silencing mark[7,33,34]. We first examined the MAT locus. Note that we cannot make definite statements about ChIP-seq signals over the "green" and "orange" reporters themselves, as the reporter cassettes harbor sequences that are duplicated 3-4 times in the genome[31], making ChIP-seq read assignment ambiguous. Overall, H3K9me2 levels at the MAT locus dropped significantly in *Δswi6,* consistent with prior work[7]; however, *swi6*$^{S18/24A}$ mutant maintained similar levels of H3K9me2 to wild-type *swi6* (**Figure 2.3B,** top). Examining the distribution more closely, at the *cenH* nucleator, only *Δswi6* showed a minor decline of H3K9me2 in some regions. To the left of *cenH,* H3K9me2 levels significantly decreased in *Δswi6*. To the right of *cenH,* H3K9me2 levels also severely declined in *Δswi6,* while in *swi6*$^{S18/24A}$ they appear to drop moderately near *mat3M*, but then recovered to wild-type levels at IR-R. When examining H3K9me3, we observed a different relationship: H3K9me3 patterns in *swi6*$^{S18/24A}$ much more closely mirrored *Δswi6*. Specifically, to the left of *cenH,* H3K9me3 dropped to an intermediate level between wild-type and *Δswi6,* while on the right of *cenH,* H3K9me3 levels closely matched *Δswi6 (***Figure 2.3B,** bottom). Importantly, this behavior of H3K9me3 is consistent with our flow cytometry results (**Figure 2.1**), where silencing is largely unaffected at "green" in *swi6*$^{S18/24A}$, while "orange" was expressed.

We wanted to further examine if the observation of H3K9me3 loss in *swi6*$^{S18/24A}$ versus wild-type *swi6* held for other genome regions. When we analyzed the subtelomeric region (*tel IIR*) we found that over the nucleation region *tlh2,* H3K9me2 levels are slightly elevated in

swi6$^{S18/24A}$, but then begin to drop ~6.4 kb to the left of *tlh2* (**Figure 2.3C,** top, red bar, and arrow). Interestingly, H3K9me3 levels drop closer to the *tlh2* nucleator than H3K9me2*;* the 95% confidence interval of wild-type and *swi6*$^{S18/24A}$ separate at the left edge of *tlh2* (**Figure 2.3C,** bottom). This observation at the *tlh2* nucleator suggests the conversion of H3K9me2 to H3K9me3 is inhibited right as heterochromatin structures exit nucleation centers. We observed the same trend at the left subtelomere of chromosome I (*tel IL*, **Figure 2.4B**). At the subtelomere, spreading distances outside nucleation sites are longer than at other loci, thus this loss of H3K9me3 just outside *tlh2* has the opportunity to manifest as an H3K9me2 spreading defect several kilobases downstream. This result is consistent with the requirement of Suv39/Clr4 methyltransferases to bind H3K9me3 for H3K9 methylation spreading[5,23]. We note that the left telomere of chromosome II contains no annotated nucleators in the published sequence. Hence, we could not observe the same trend there. (*tel IIL,* **Figure 2.4C**).
A similar defect in H3K9me3 spreading also occurs at the pericentromere (*cenII*), specifically, from the outer repeat (*otr*) into the inner repeat (*imr*) (**Figure 2.3D**, bottom versus top). However, the distances are likely too short from nucleation centers in *otr* to observe a resulting loss of H3K9me2 (**Figure 2.3D**). We note no distinguishable differences in H3K9me2 and H3K9me3 at *mei4*, a well-studied heterochromatin island (**Figure 2.4A**).

Together, our ChIP-seq data show that *swi6*$^{S18/24A}$ is deficient in the conversion of H3K9me2 to me3 outside nucleation centers, which results in loss of silencing and ultimately, the loss of H3K9me2 spreading, as evident for the subtelomere.

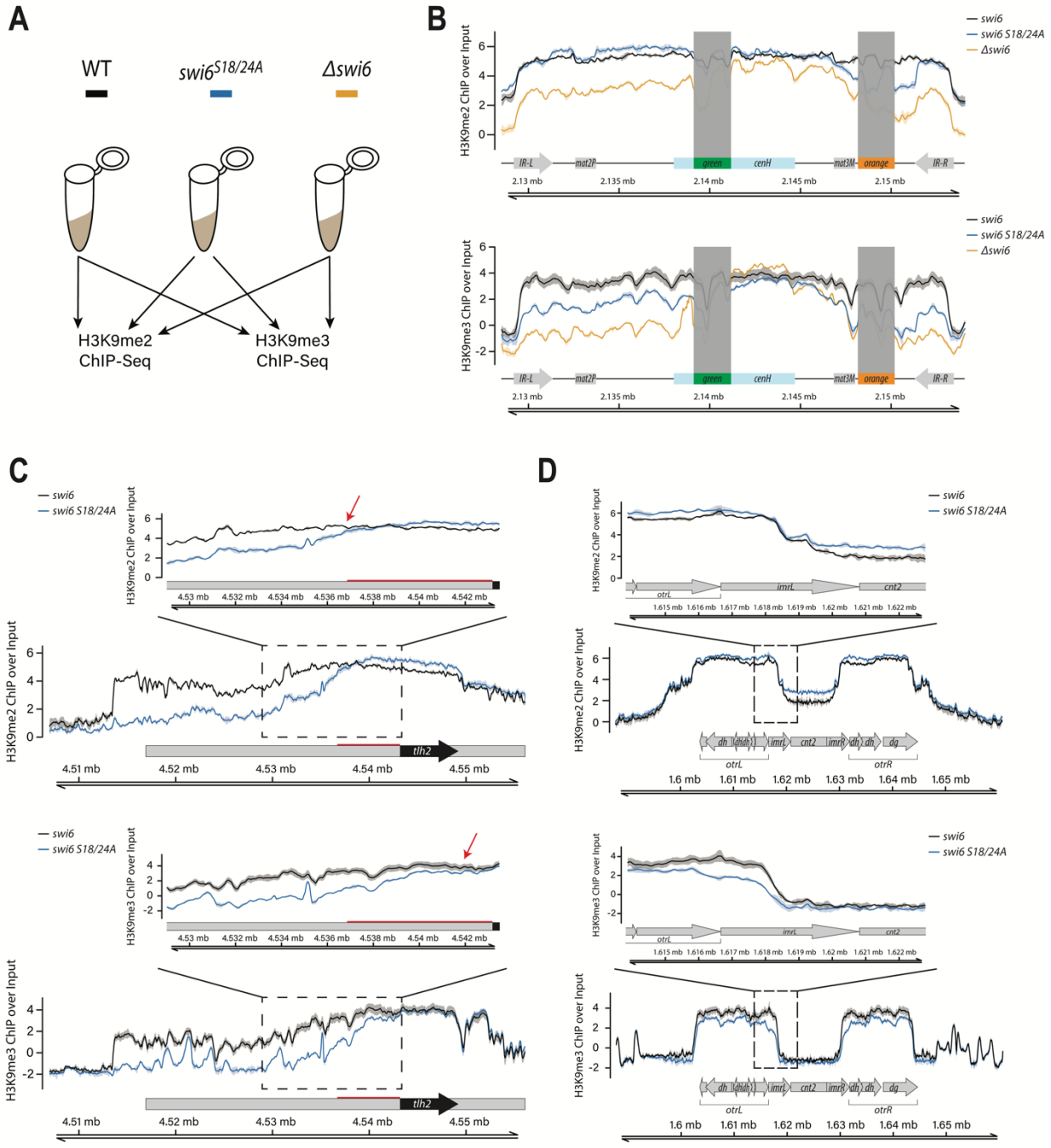

Figure 2.3 Conversion from H3K9me2 to H3K9me3 is compromised outside nucleation centers in S18 and S24 Swi6 mutants. A. Overview of the ChIP-seq experiments. **B-D.** ChIP-seq signal visualization plots. The solid ChIP/input line for each genotype represents the mean of three repeats, while the shading represents the 95% confidence interval. **B.** Plots of H3K9me2 (TOP) and H3K9me3 (BOTTOM) ChIP signal over input at the MAT *ΔREIII* HSS mating type locus for wild-type (black), *swi6*$^{S18/24A}$ (blue), and *Δswi6* (gold). Signal over "green" and "orange" reporters are greyed out, as reads from these reporters map to multiple locations within the reference sequence, as all reporters contain control elements derived from the *ura4* and *ade6* genes. (Figure caption continued on the next page.)

(Figure caption continued from the previous page.)
C. H3K9me2 (TOP) and H3K9me3 (BOTTOM) plots as in A. for subtelomere IIR for wild-type and *swi6*$^{S18/24A}$. The red bar on the H3K9me2 plots indicates the distance from *tlh2* to where H3K9me2 levels drop in *swi6*$^{S18/24A}$ relative to wild-type. Inset: a zoomed-in view proximal to *tlh2* is shown for H3K9me2 and me3. The red arrows in the insets indicate the point of separation of the 95% confidence intervals, which is significantly further telomere proximal for H3K9me3. **D.** H3K9me2 (TOP) and H3K9me3 (BOTTOM) plots as in A. for centromere II for wild-type and *swi6*$^{S18/24A}$. Inset: the left side of the pericentromere.

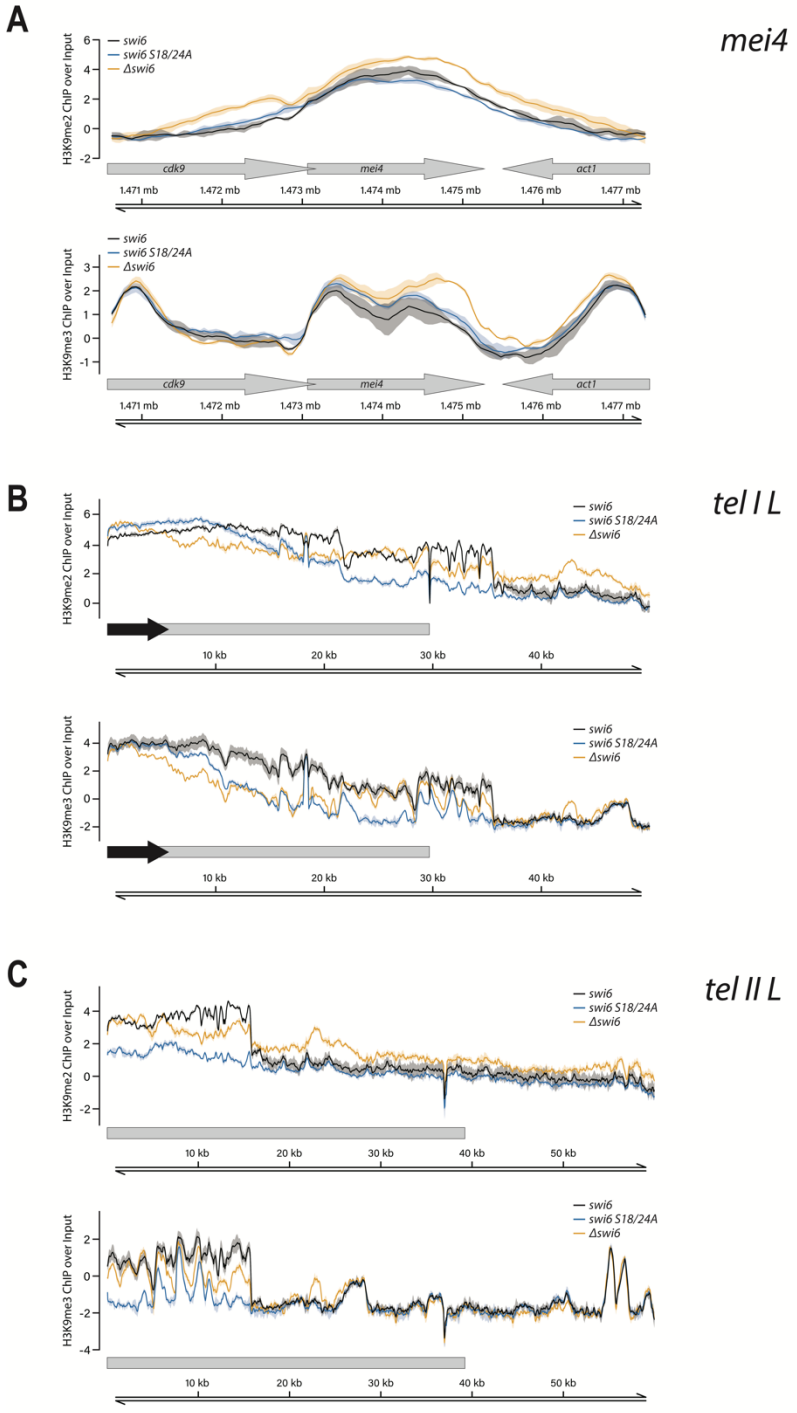

Figure 2.4 H3K9me2 and H3K9me3 ChIP-seq plots in additional genomic loci in wild-type swi6, *swi6*$^{S18/24A}$, and *Δswi6*. A. H3K9me2 (TOP) and H3K9me3 (BOTTOM) plots as in Figure 2.3 at *mei4* for wild-type *swi6*, *swi6*$^{S18/24A}$, and *Δswi6*. (Figure caption continued on the next page.)

(Figure caption continued from the previous page.)
B. H3K9me2 (TOP) and H3K9me3 (BOTTOM) plots as in Figure 2.3 at *tel IL* for wild-type *swi6*, *swi6*$^{S18/24A}$, and *Δswi6*. **C.** H3K9me2 (TOP) and H3K9me3 (BOTTOM) plots as in Figure 2.3 at *tel IIL* for wild-type *swi6*, *swi6*$^{S18/24A}$, and *Δswi6*.

Swi6 phosphorylation increases oligomerization and decreases nucleosome affinity.

Next, we wanted to pinpoint the biochemical mechanisms that can account for the spreading defects in *swi6*$^{S18/24A}$ (**Figure 2.1G, Figure 2.3**). HP1 oligomerization has been linked to spreading[12]. In turn, HP1's intranuclear dynamics have been linked to how it engages chromatin[35–38]. We thus probed if and how phosphorylation may impact these two properties of Swi6.

We used Size Exclusion Chromatography followed by Multi-Angle Light Scattering (SEC-MALS) to probe oligomerization, and fluorescence polarization to quantify H3K9me3 peptide and nucleosome binding. To produce phosphorylated Swi6 (pSwi6), we co-expressed Swi6 with Caesin Kinase II (CKII) in *E. coli* (**Figure 2.5A**). We used 2-dimensional Electron Transfer Dissociation Mass Spectrometry (2D ETD-MS) to identify which residues in pSwi6 are phosphorylated and used unphosphorylated Swi6 (unpSwi6) as a control (**Figure 2.5B**). We found that only pSwi6, and not unpSwi6, has detectable phosphorylated peptides. The residues phosphorylated in pSwi6 include several that were identified *in vivo* (**Figure 2.1A,** S18, S24, S46, S52, S117, S212, S220 but not S192) and some additional sites not previously identified (S43, S45, S165, S224, S227). This detection of additional CKII target sites is likely because of the higher sensitivity achieved in our 2D-ETD-MS experiments from purified protein: 1. 2D-ETD-MS better preserves phosphorylation sites compared to other methods and is highly sensitive. 2 Pure, *in vitro*-produced protein of high yield is likely to result in more detection events than *in vivo*-derived protein.

SEC-MALS traces of uncrosslinked pSwi6 and unpSwi6 reveal both proteins are estimated to be of similar dimer mass, 90.8 kDa and 100.4 kDa respectively (**Figure 2.6A**). However, pSwi6 elutes before Swi6, a trend similar to phosphorylated HP1α[13]. There is also a small shoulder in the pSwi6 trace, indicating a minor fraction of higher-order oligomers (**Figure 2.6A**, grey arrow). As previously published[12], Swi6 crosslinking leads to the appearance of

higher molecular weight species. We observed that crosslinked Swi6 and pSwi6 elute as apparent dimers (93.4 and 86.2 kDa, respectively) and tetramers (210.6 and 180.8 kDa, respectively) (**Figure 2.5D**). However, only pSwi6 additionally forms octamers (365.2kDa) and possibly even larger oligomers, as indicated by a broad shoulder (**Figure 2.5D**).

We next quantified the binding of pSwi6 to H3K9me0 and H3K9me3 peptides by fluorescence polarization (**Figure 2.5D**). pSwi6 binds to H3K9me0 and H3K9me3 peptides with affinities (K_d) of 227.4μM and 2.45μM, respectively, revealing a ~93X specificity for H3K9me3 (**Figure 2.5F**). While we could not determine the H3K9me0 peptide K_d for unpSwi6, the K_d for the H3K9me3 peptide was 8.17 μM (**Figure 2.5D**, **F**). Previously, the specificity for unpSwi6 was reported at ~130X[12], thus indicating little difference in H3K9me3 peptide specificity between the two proteins.

We next probed how phosphorylation affects nucleosome binding. We performed fluorescence polarization with fluorescently labeled nucleosomes that are unmethylated (H3K9me0) or trimethylated ($H3K_c9me3$)[39,12]. Phosphorylation had no impact on the specificity for the H3K9me3 mark, consistent with the peptide observation (19.4X, vs. 19X for unpSwi6 or pSw6, respectively, **Figure 2.5E**, **F**).

However, we observe a 12X difference in affinity to the nucleosome overall between pSwi6 and Swi6 (**Figure 2.5F**). The $H3K_c9me3$ nucleosome affinity is 0.12 μM and 1.45 μM for unpSwi6 and pSwi6, respectively, while the H3K9me0 affinity is 2.33 and 27.5 μM, respectively. We note the affinity of pSwi6 to the $H3K_c9me3$ nucleosome is similar to its affinity to the H3K9me3 peptide, binding only 1.7X tighter to the $H3K_c9me3$ nucleosome (1.45μM vs. 2.45μM). Instead, and consistent with previous results, unpSwi6 binds 68X more tightly to the nucleosome than to the tail (8.17 μM for the H3K9me3 tail versus 0.12μM for H3Kc9me3), which is thought to arise from additional contacts beyond the H3 tail on the nucleosome. Why would a 12X lower affinity towards the nucleosome substrate be advantageous for pSwi6's function in spreading (**Figure 2.1**, **2.3**)? In the literature, the cellular abundance of Swi6 is

measured at 9000- 19,400 molecules per cell[40,41]. The estimated fission yeast nuclear volume of ~7mm^3 [42,43] then yields an approximate intranuclear Swi6 concentration of ~2.1 -4.6μM. Given our measured nucleosome K_ds (**Figure 2.5F**), the intranuclear concentration of unpSwi6 would theoretically be above its K_d for both H3K9me0 and me3 nucleosomes. The concentration of pSwi6 would exceed its K_d for H3K_c9me3 but be significantly below (~10X) its K_d for H3K9me0 nucleosomes. We cannot assume the same fraction of bound nucleosome from *in vitro* measurements applies *in vivo*, because nucleosome concentrations in the cell (~10μM based on accessible genome size and average nucleosome density[44,45]) greatly exceed what is used in a binding isotherm. We can use a quadratic equation[46] (see methods) appropriate for these *in vivo* regimes instead of a typical K_d fit to estimate the fraction bound. As only 2% of the *S. pombe* genome is heterochromatic, we approximate the total nucleosome concentration (10μM) to reflect unmethylated nucleosomes. The small, methylated nucleosome pool will mostly be bound by Swi6 irrespective of the phosphorylation state. However, we estimate that only 5% of unmethylated nucleosomes would be bound by pSwi6, while this would be ~16% for unpSwi6. At the high end of the Swi6 concentration estimate, this fraction bound would increase to 30% of unmethylated nucleosomes. Further, we expect enhanced oligomerization of pSwi6 on heterochromatin to reduce the free Swi6 pool (see discussion). Therefore, we predict that the main function of phosphorylation is to limit the partitioning of Swi6 into the unmethylated pool, confining it to heterochromatin.

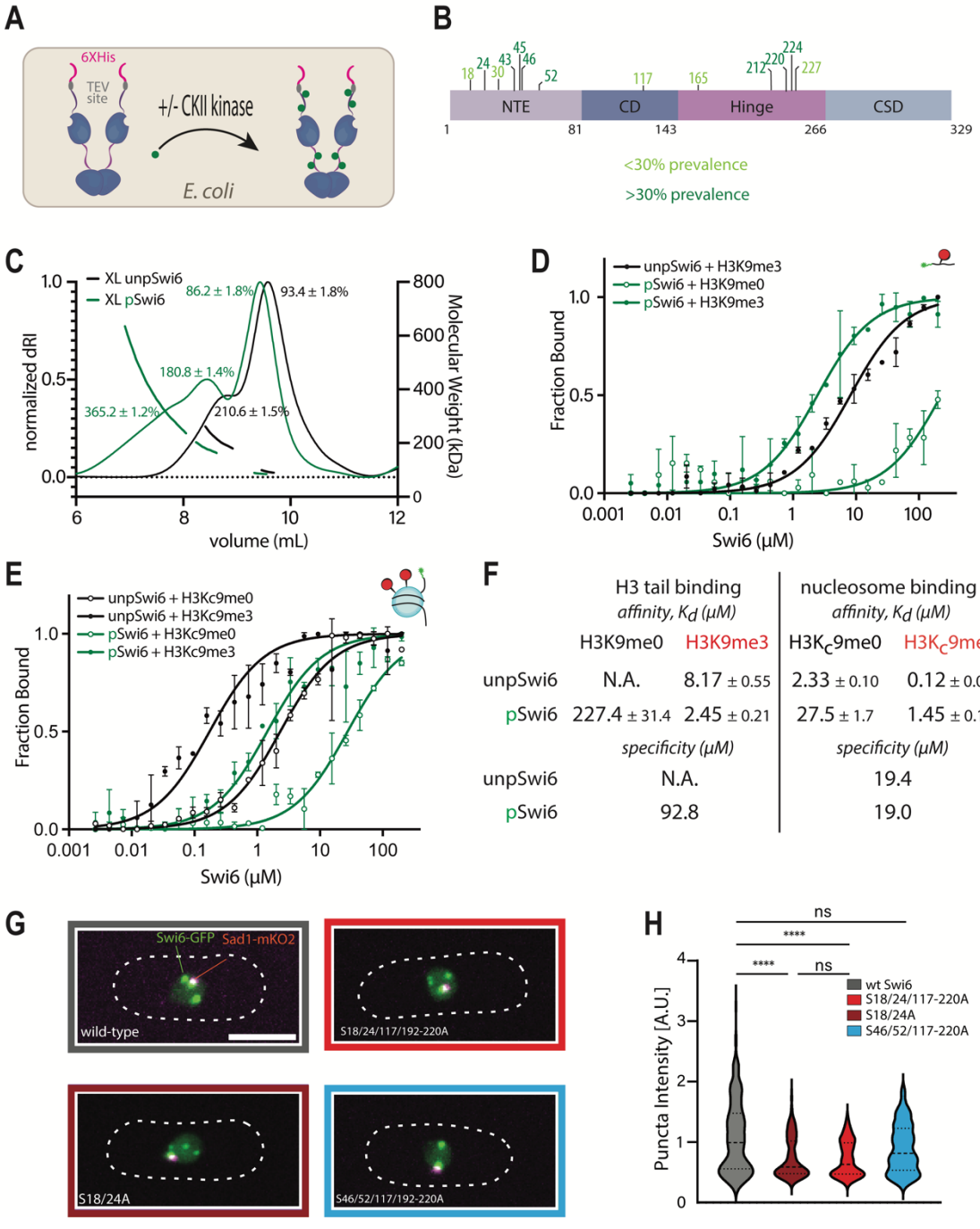

Figure 2.5 Swi6 phosphorylation increases oligomerization and decreases nucleosome binding, without affecting specificity. A. Production of phosphorylated Swi6 (pSwi6) in *E. coli.* Casein Kinase II (CKII) is co-expressed with Swi6. After lysis and purification, the 6Xhis-tag is removed from the pSwi6 or unpSwi6 protein. **B.** Mass Spectrometry on pSwi6. Shown is a domain diagram of Swi6. Phosphorylation sites identified in pSwi6 by 2D-ETD-MS are indicated and grouped by detection prevalence in the sample. **C.** Size Exclusion Chromatography followed by Multi-Angle Light Scattering (SEC-MALS) on EDC/NHS cross-linked unpSwi6 (black) and pSwi6 (green). (Figure caption continued on the next page.)

(Figure caption continued from the previous page.)
Relative refractive index signals (solid lines, left y-axis) and derived molar masses (lines over particular species, right y-axis) are shown as a function of the elution volume. [Swi6] was 100μM. **D.** Fluorescence polarization (FP) with fluorescein (star)- labeled H3 tail peptides (1-20) and pSwi6 (green) or unpSwi6 (black) for H3K9me0 (open circles) and H3K9me3 (filled circles) is shown. Error bars represent standard deviation. Binding was too low to be fit for unpSwi6 and H3K9me0 peptides. **E.** FP with H3K9me0 (open circles) or $H3K_c9me3$ (MLA, filled circles) mononucleosomes. Fluorescein (green star) is attached by a flexible linker at one end of the 147 bp DNA template. For D.&E., the average of three independent fluorescent polarization experiments for each substrate is shown. Error bars represent standard deviation. **F.** Summary table of affinities and specificities for D. and E. **G.** Representative maximum projection live microscopy images of indicated Swi6-GFP / Sad1-mKO2 strains. **H.** Analysis of signal intensity in Swi6-GFP foci in indicated strains. Wt Swi6, n=242; $Swi6^{S18/24A}$, n=251; $Swi6^{S18/24/117-220A}$, n=145; $Swi6^{S46/52/117-220A}$, n=192. n, number of foci analyzed.

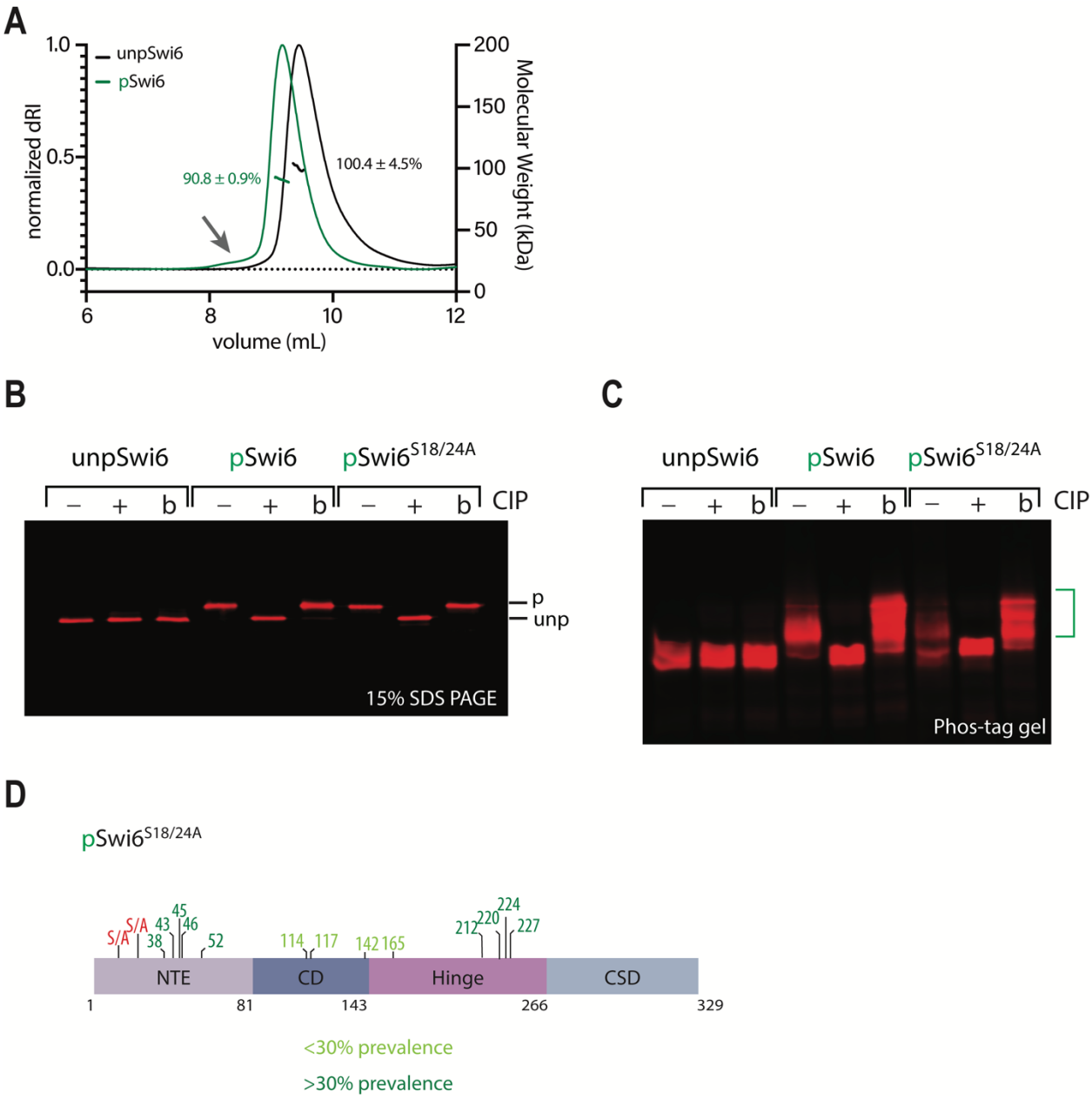

Figure 2.6 Characterization of recombinant pSwi6. A. Size Exclusion Chromatography followed by Multi-Angle Light Scattering (SEC-MALS) on uncrosslinked unpSwi6 (black) and pSwi6 (green). Relative refractive index signals (solid lines, left y-axis) and derived molar masses (lines over particular species, right y-axis) are shown as a function of the elution volume. A migration shift is apparent in pSwi6, as well as a small shoulder of higher molecular weight species (arrow). **B.** Calf Intestine Phosphatase (CIP) treatment of Swi6 examined in a 15% SDS-PAGE gel. unpSwi6, pSwi6, or pSwi6$^{S18/24A}$ were treated with (+) or without (-) CIP or with heat-inactivated CIP (b). **C.** CIP treatment of Swi6 examined in a Phos-tag gel as in A. Blots of both gels were probed with an anti-Swi6 polyclonal antibody. **D.** Mass Spectrometry on pSwi6$^{S18/24A}$. Shown is a domain diagram of Swi6$^{S18/24A}$. Phosphorylation sites identified in pSwi6 $^{S18/24A}$ by 2D-ETD-MS are indicated and grouped by detection prevalence in the sample.

One test of this prediction would be altered localization of wild-type and phosphorylation defective Swi6 versions in the fission yeast nucleus. Across species, HP1 homologs have been shown to localize into heterochromatic foci *in vivo* and form LLPS droplets *in vitro* [13,14,16,35]. Specifically, phosphorylation of the NTE in human HP1α is one driver of heterochromatin foci formation[13,36]. We investigated whether the loss of phosphorylation sites that impair heterochromatin spreading (**Figure 2.1**, **2.3**) impacted partitioning between heterochromatin foci and regions outside these foci, likely representing H3K9 unmethylated nucleosomes. We C-terminally tagged wild-type *swi6* and phospho-serine mutants at the native locus with super fold-GFP (Swi6-GFP), as an N-terminal tag disrupt Swi6 dimerization and oligomerization[25]. We crossed these strains into a background containing *sad1*:mKO2, a spindle pole body (SPB) marker (**Figure 2.8A**). We chose this background, as Sad1 denotes the position of pericentromeric heterochromatin[47,48] and can help orient other heterochromatin sites relative to it. We examined the following SF-GFP tagged mutant variants: *swi6*$^{S18/24A}$, *swi6*$^{S46/52A}$, *swi6*$^{S46/52/117\text{-}220A}$ (S18/S24 available), *swi6*$^{S18/24/117\text{-}220A}$ (S46/S52 available) (**Figure 2.1G-I**) and imaged these strains by confocal microscopy (**Figure 2.5G**, **Figure 2.8B**). Largely, these mutations do not impact either Swi6 accumulation (**Figure 2.8C**), nuclear foci number (**SFigure 2.8D**), or position of the foci relative to the SPB[49] (**Figure 2.8E**, **F**).

We next quantified the accumulation of Swi6-GFP in foci. Unlike foci number or spatial arrangement, the average foci intensity for Swi6-GFP strains carrying the S18/24A mutations is significantly decreased relative to wild-type Swi6-GFP (**Figure 2.5H**), while the nucleoplasmic signal increases. Because total Swi6-GFP levels do not change in these mutants (**Figure 2.8C**), this result indicates that Swi6$^{S18/24A}$-GFP and Swi6$^{S18/24/117\text{-}220A}$ -GFP molecules partition away from heterochromatin foci. This finding is consistent with our prediction based on our *in vitro* measurements and implies that Swi6 molecules that cannot normally be phosphorylated partition onto unmethylated nucleosomes.

Swi6 phosphorylation facilitates the conversion of H3K9me2 to me3 by Clr4

As unmethylated nucleosomes are Clr4's substrates, another prediction emerges. Since unpSwi6 is more likely to bind unmethylated nucleosomes, Swi6 phosphorylation mutants may interfere with Clr4 substrates, which could explain the inhibition of H3K9me2 to me3 conversion (**Figure 2.3**). However, for Swi6 phosphorylation to prevent such inhibition, the Swi6 cellular pool would have to be mostly in the phosphorylated state. To test this, we asked which fraction of Swi6 molecules in the cell are phosphorylated at S18 and S24. We addressed this question by a western blot approach, using two antibodies: a polyclonal Swi6 antibody[25] to detect all Swi6 molecules and a phospho-serine antibody specific to phosphorylation at S18 and S24 (top blot vs. bottom blot, respectively, **Figure 2.7A**). A standard curve of recombinant pSwi6 allowed us to quantify the total pool of Swi6 molecules vs. those phosphorylated at S18 and S24. The *swi6*$^{S18/24A}$ mutant control shows these phospho-serine antibodies are indeed specific (**Figure 2.7A**). We showed that 70-100% of cellular Swi6 is phosphorylated at S18 and S24 (**Figure 2.7A** and **Figure 2.9A**).

We next tested if Swi6 phosphorylation directly impacted the ability of Clr4 to produce H3K9me3. We incubated pSwi6 or unpSwi6 with Clr4 and monitored the conversion of the H3K9me2 substrate to H3K9me3 under single turnover conditions[23] (**Figure 2.7B**).
We observed that the presence of unpSwi6 inhibits the conversion of H3K9me2 to H3K9me3 in a concentration-dependent manner, but that this inhibition is significantly alleviated by pSwi6 (**Figure 2.7C** and **Figure 2.9B, C**). When normalizing to H4 and fitting H3K9me3 to k_{obs}, Clr4 methylation rates are significantly slowed in the presence of unpSwi6, while pSwi6 reduces this inhibition (**Figure 2.7D**, **E**).

While these data could explain the H3K9me3-spreading defect, we observe for *swi6*$^{S18/24A}$ (**Figure 2.3**), our *in vitro*-produced pSwi6 is phosphorylated at multiple residues. Given that S18 and S24 only represent around 1/6 of the detected phosphorylation sites (**Figure 2.5B**), we cannot necessarily conclude whether the biochemical phenotypes we observe

depend on S18 and S24 phosphorylation. To examine this, we expressed and purified a phospho-mutant protein, pSwi6$^{S18/24A}$, in which S18 and S24 are mutated to alanines and co-expressed it with CKII. pSwi6$^{S18/24A}$ is still phosphorylated to a similar degree as pSwi6, which is apparent by the similar gel migration shift observed for both proteins (**Figure 2.6B**, **C**). Upon phosphatase treatment, pSwi6$^{S18/24A}$ and pSwi6 adopt the same migration pattern as unpSwi6 (**Figure 2.6B**, **C**). 2D ETD-MS analysis of pSwi6$^{S18/24A}$ additionally confirmed a similar phosphopeptide pattern to pSwi6, though with small changes in phosphopeptide prevalence (**Figure 2.6D**).

We examined nucleosome affinity of pSwi6$^{S18/24A}$ compared to pSwi6 via fluorescence polarization and found that pSwi6$^{S18/24A}$ shows increased affinity towards both the H3K9me0 and K_c9me3 nucleosomes, 4.5 and 2.6X, respectively (**Figure 2.7F**). This result is consistent with S18 and S24 phosphorylation sites acting to modulate Swi6's chromatin affinity. However, since the change in affinity for pSwi6$^{S18/24A}$ is less than the 12X loss observed for unpSwi6 vs. pSwi6, this implies that other phosphoserines also contribute to lowering nucleosome affinity. Overall, this data suggests a model whereby Swi6 NTE phosphorylation, particularly at S18 and S24, partitions Swi6 away from binding the unmethylated substrate of Clr4 *in vivo,* which is likely enhanced by increased Swi6 oligomerization at heterochromatin sites. Together, both reduced affinity and oligomerization mechanisms promote the H3K9me3 spreading reaction.

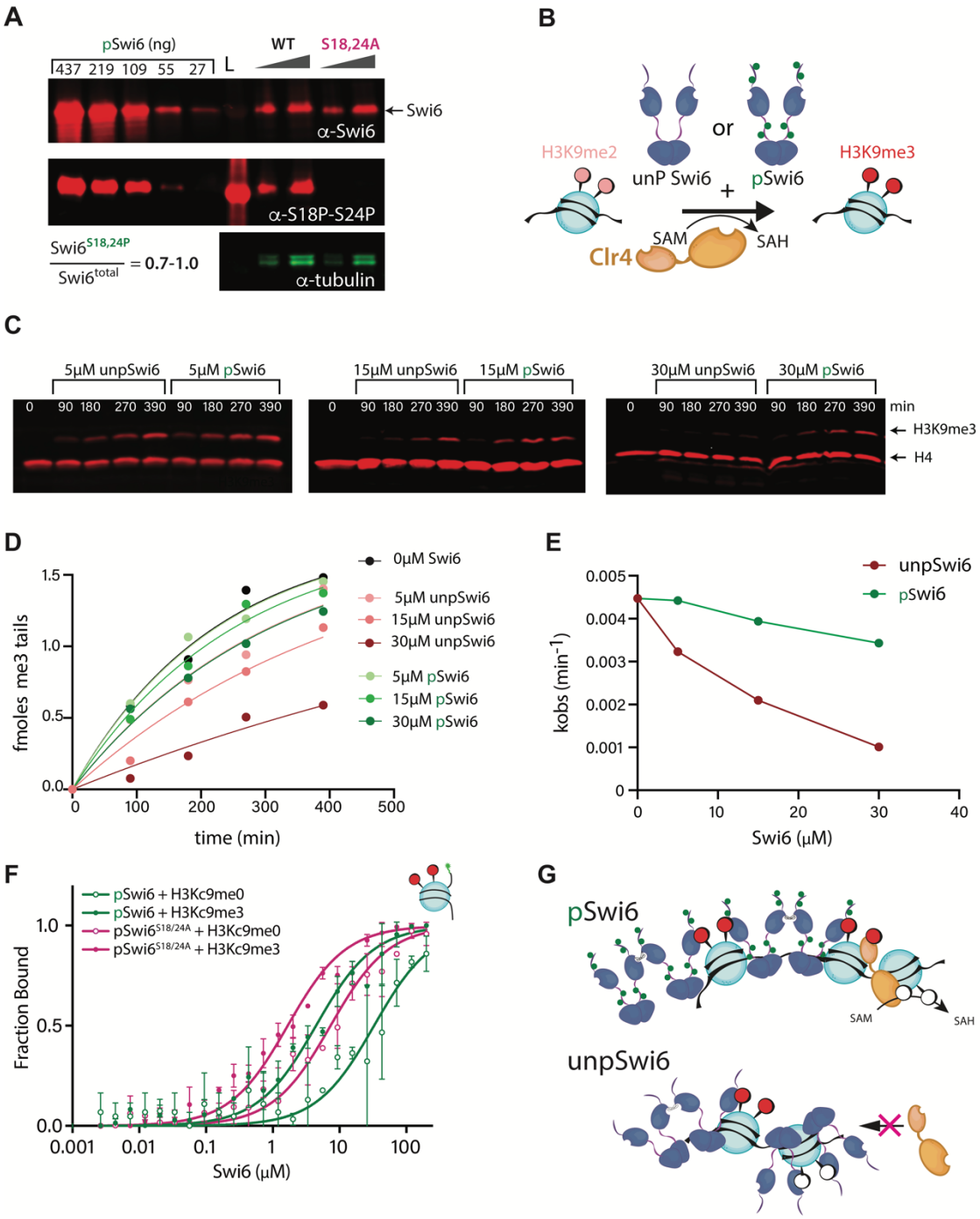

Figure 2.7 Swi6 phosphorylation mitigates inhibition of the Clr4-mediated conversion of H3K9me2 to H3K9me3. A. Most Swi6 molecules in the cell are phosphorylated at S18 and S24. Quantitative western blots against total Swi6 and phosphorylated Swi6 at S18/S24. A standard curve of pSwi6 is included in both blots. Total protein lysates from wild-type *swi6* and *swi6*$^{S18/24A}$ strains were probed with a polyclonal anti-Swi6 antibody (α-Swi6) or an antibody raised against a phosphorylated S18/S24 peptide (α-S18P-S24P). α-tubulin was used as a loading control. One of two independent experiments is shown. **B.** Experimental scheme to probe the impact of Swi6 on H3K9 trimethylation. **C.** Quantitative western blots on the time-dependent formation of H3K9me3 from H3K9me2 mononucleosomes (Figure caption continued on the next page.)

(Figure caption continued from the previous page.)
in the presence of pSwi6 or unpSwi6. The same blots were probed with α-H3K9me3 and α-H4 antibodies as a loading and normalization control. **D.** Single exponential fits of production of H3K9me3 tails over time for indicated concentrations of unpSwi6 or pSwi6. **E.** plot of k_{obs} vs. [Swi6] (μM). **F.** Fluorescence polarization with H3K9me0 (open circles) or H3K_c9me3 (MLA, filled circles) (Figure caption continued on the next page.)(Figure caption continued from the previous page.) mononucleosomes as in Figure 3E., with pSwi6 (green) or pSwi6$^{S18/24A}$ (magenta). Relative K_d values in Table 1. Error bars represent standard deviation. **G.** Model of the impact of pSwi6 on Clr4 activity. Top: pSwi6 does not engage with K3K9me0 nucleosomes, clearing the substrate for Clr4, and has reduced interactions with the nucleosome core. Bottom: Swi6 binds H3K9me3 and me0 nucleosomes, occluding Clr4 access.

Table 1: Binding affinities and specificity for fluorescence polarization curves in Fig. 2.7F. Mononucleosome binding affinities (K_d value, μM) and specificity for pSwi6 and pSwi6$^{S18/24A}$.

	Mononucleosome binding	
	affinity, K_d (μM)	
	H3K_c9me0	H3K_c9me3
pSwi6	7.48 ± 1.07	1 ± 0.1
pSwi6$^{S18/24A}$	1.67 ± 0.15	0.38 ± 0.003
	specificity (μM)	
pSwi6	7.48	
pSwi6$^{S18/24A}$	4.39	

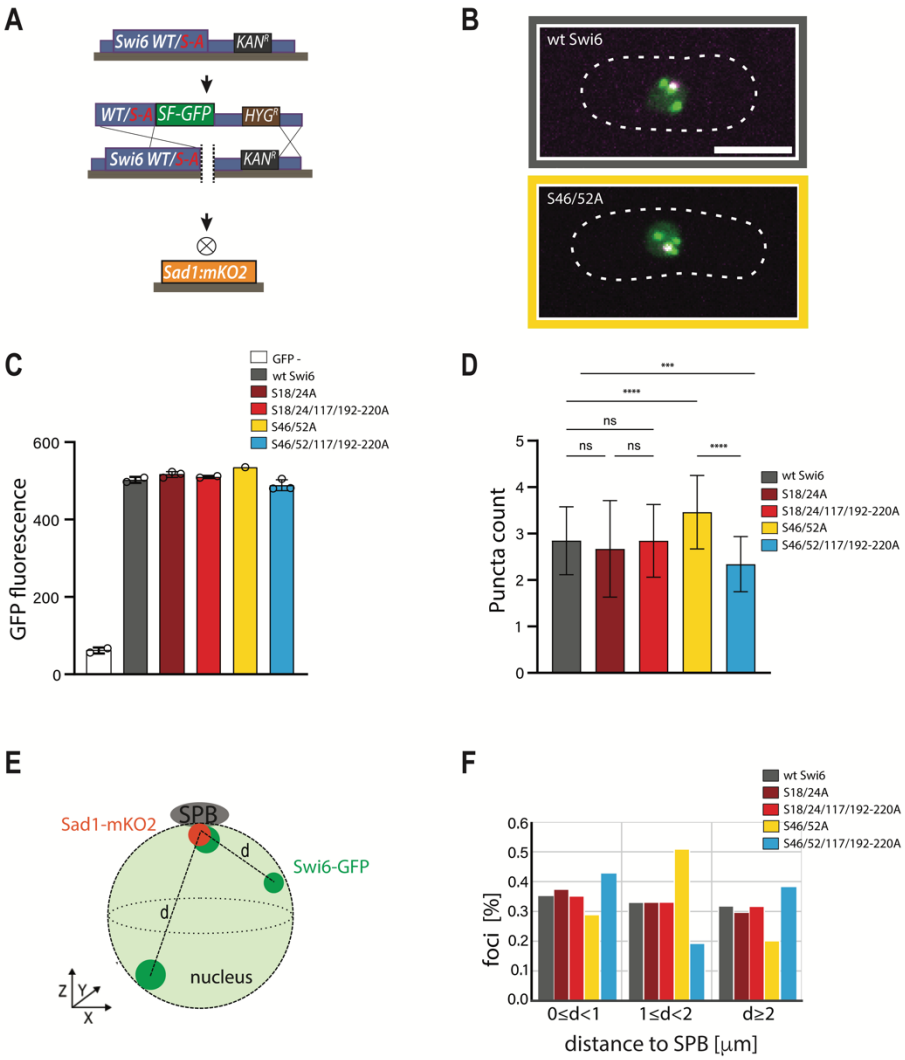

Figure 2.8 Analysis of Swi6-GFP heterochromatin foci number and spatial distribution. **A.** Strategy for production of GFP-tagged *swi6* S-A mutants in the *sad1:mKO2* background. The wildtype *swi6* or S-A mutant gene from Figure 2A was cut with CRISPR/Cas9, and the break was repaired with a cassette containing a super-folder GFP, *swi6* 3' sequence homology, and a HygMX cassette. **B.** Representative maximum projection live microscopy images of indicated Swi6$^{S46/52A}$-GFP /Sad1-mKO2 compared to the wild-type strain. **C.** Quantification of Swi6-GFP signals by flow cytometry. The GFP signal of independent wild-type or S-A mutant isolates compared to GFP- cells as measured by flow cytometry. **D.** Distribution of nuclear foci in nuclei of indicated strains represented as relative frequency. Wt Swi6-GFP , n=85; Swi6$^{S18/24A}$-GFP, n=94; Swi6$^{S18/24/117-220A}$-GFP, n=50; Swi6$^{S46/52/117-220A}$-GFP, n=82. **E.** distribution of Swi6-GFP heterochromatin foci relative to Sad1-mKO2. overview: center-to-center distances were measured in 3D from the peri-spindle pole body Sad1-mKO2 signal to all Swi6-GFP foci identified in each nucleus. **F.** relative frequency histogram binning the distribution of Sad1-mKO2 to Swi6-GFP foci distances in indicated strains.

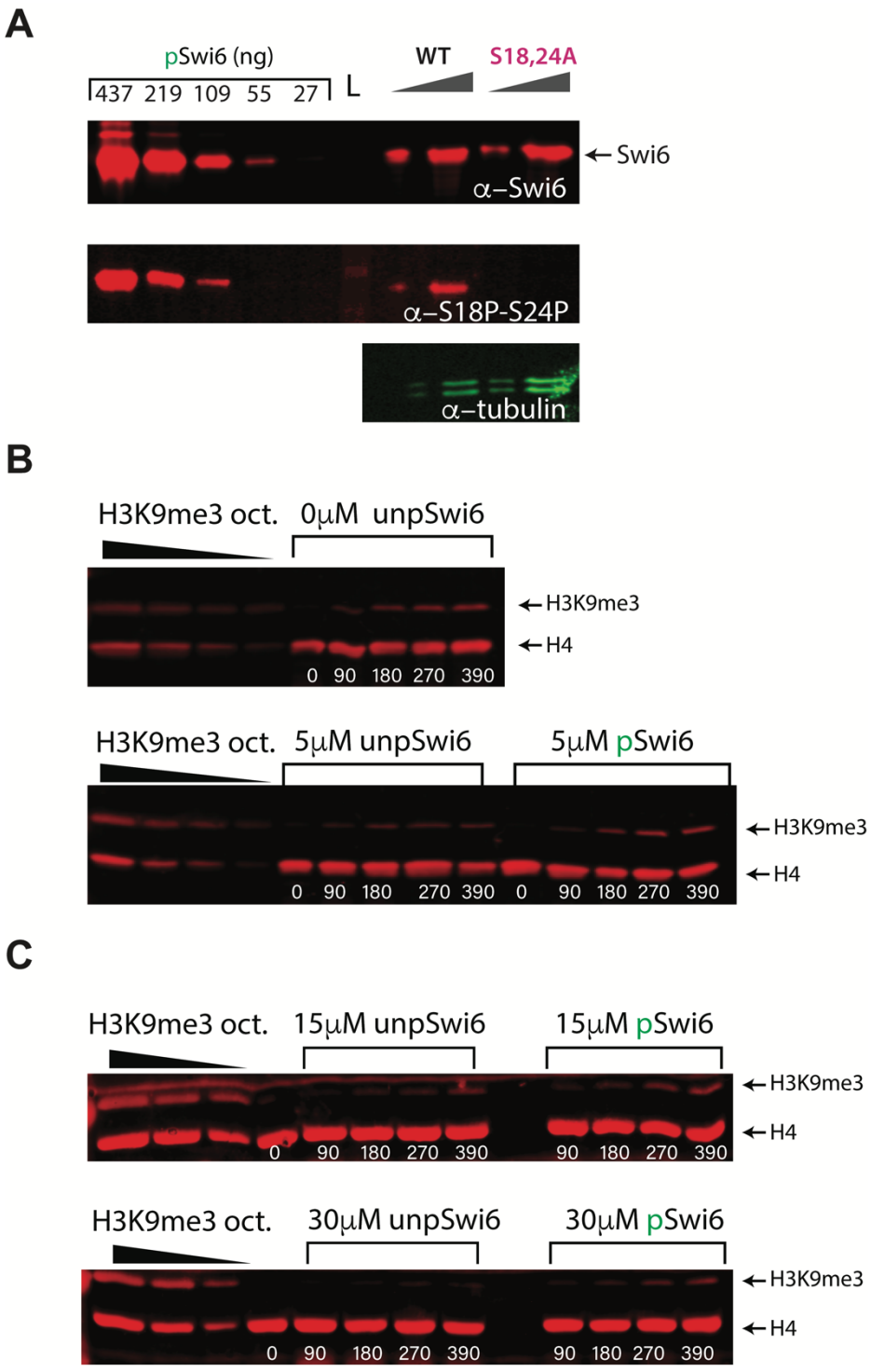

Figure 2.9 Additional replicates of Swi6 westerns from cell lysates and nucleosome trimethylation. A. Independent repeat of α-Swi6 and α-S18P-S24P westerns as in Figure 2.7A. **B.** A repeat of quantitative western blots querying time-dependent formation of H3K9me3 from H3K9me2 mononucleosomes in the presence of pSwi6 or unpSwi6 (0 and 5μM Swi6). (Figure caption continued on the next page.)

(Figure caption continued from the previous page.)
C. A repeat of quantitative western blots querying time-dependent formation of H3K9me3 from H3K9me2 mononucleosomes in the presence of pSwi6 or unpSwi6 (15μM and 30μM Swi6). B and C. Swi6 concentration time courses were collected at the same time; westerns were run on separate days.

2.3 Discussion

Previous work[27] identified key Swi6 phosphoserines that regulate transcriptional gene silencing. In this work, we find that Swi6 phosphoserines 18 and 24 are required for heterochromatin spreading, but not nucleation (**Figure 2.1**). Swi6 phosphorylation promotes oligomerization, and tunes Swi6's overall chromatin affinity to a regime that allows Clr4 to access its substrate (**Figure 2.5**), facilitating the conversion of dimethyl H3K9 to the repressive and spreading-promoting trimethyl H3K9 state (**Figure 2.7**). This modulation of chromatin affinity *in vivo* restricts Swi6 to heterochromatin foci (**Figure 2.5, Figure 2.8**), which suggests that phosphorylation of HP1 molecules may be required for their concentration into the heterochromatic compartment. Three central themes emerge from this work:

Swi6 phosphorylation decreases chromatin affinity, but not specificity.

Phosphorylation of HP1s regulates its affinity with itself[13], DNA[30,36], and chromatin[30,36], but in manners that are homolog-specific. For example, phosphorylation in the NTE of HP1α induces LLPS, but not for HP1a in *Drosophila*, where phosphorylation instead regulates chromatin binding[16,50,51]. Underlying this may be that CKII target sequences are not conserved across HP1s, for example, HP1α is phosphorylated in a cluster of 4 serines at the NTE (S11-14)[29], HP1a only at S15 in the NTE, and S202 C-terminal to the CSD[50], whereas we report here Swi6 is phosphorylated by CKII in the NTE, CD, and hinge (**Figure 2.5B**).

Phosphorylation increases the affinity towards H3K9me3 and H3K9me0 peptides both for Swi6 (**Figure 2.5D**) and HP1α[36]. However, the impact on nucleosome specificity is different across species. Our data here shows that phosphorylation of Swi6 does not affect its specificity for both H3K9me0 and H3Kc9me3 nucleosomes (**Figure 2.5E**, **F**), but phosphorylation of HP1α and HP1a was reported to increase its specificity for H3K9me3 nucleosomes[13,30]. Instead, Swi6 phosphorylation decreases overall nucleosome affinity for unmethylated and H3Kc9me3 nucleosomes to a similar degree, 11.8X and 12X respectively, in contrast to HP1α[30,52]. What

may explain these differences? Internal interactions between the NTE, CD, hinge, and CSD work together to drive nucleosome binding[17,25]. We speculate that these domain interactions are differentially impacted by 1. the unique phosphorylation patterns in different HP1 orthologs (see above) and 2. divergence in Swi6 amino acid sequence and size of the NTE and hinge that harbor most CKII target sites. Both these differences result in unique outcomes with respect to nucleosome specificity and affinity in different HP1 orthologs. The reduction in affinity is likely based on the loosening of the contacts by the Swi6 hinge and CSD with the histone octamer core and DNA[17].

This overall decrease in affinity partitions pSwi6 in a different way than unpSwi6, restricting access of pSwi6 to chromatin inside nuclear foci. This is supported by our imaging data (**Figure 2.5**, **Figure 2.8**) but is also consistent with data from human HP1α[36] and *in vivo* diffusion measurements in the *swi6 sm-1* mutant. This mutant likely disrupts NTE phosphorylation and shows greater residence outside heterochromatin[37]. Further, it is likely that increased oligomerization of pSwi6 additionally strengthens this partitioning onto heterochromatin (next section). A separate consequence of this affinity decrease is the relief of competition with Clr4 for the nucleosome substrate (**Figure 2.7**, see third section below).

Swi6 phosphorylation increases oligomerization.

Swi6 has been shown to form dimers and higher-order oligomers. Swi6 oligomerization across chromatin has been linked to heterochromatin spreading *in vivo*[12]. Here, we show that phosphorylation increases the fraction of oligomeric states, revealing octamers and possibly higher molecular weight species (**Figure 2.5**). As Swi6 exists in a closed dimer that inhibits the spreading competent state, or an open dimer that promotes oligomerization[25]. One way pSwi6 could form higher molecular weight oligomers is by phosphorylation shifting the equilibrium from the closed dimer to the open dimer[25]. We speculate the following thermodynamic consequence of phosphorylation on the nuclear Swi6 pool: Oligomerization will be driven at sites of high Swi6

accumulation, which is likely near its high-affinity H3K9me3 nucleosome target. If this is true, oligomerization will reduce the pool of free Swi6 available to engage unmethylated nucleosomes even further, and below the theoretical level we described above (~5%).

HP1 proteins, like Swi6, form foci *in vivo,* which are associated with condensate formation, rooted in HP1 oligomerization[13,16,17]. The reduction of GFP-Swi6$^{S18/24A}$ in nuclear foci we observe (**Figure 2.5**) may be due to defects in condensate formation, or simply that fewer Swi6 molecules are available to form heterochromatic condensates. As discussed above, we expect defects in phosphorylation to steer Swi6 toward unmethylated chromatin sites. The reduction of GFP signal in Swi6$^{S18/24A}$ mutant foci may thus be due to losing Swi6 molecules to the nucleoplasmic space.

Phosphorylation of Swi6 enables H3K9 trimethylation by Clr4.

Achieving H3K9 trimethylation is essential for both gene silencing and heterochromatin spreading by Suv39/Clr4 enzymes[5,23]. For heterochromatin spreading, this is due to the positive feedback loop within Suv39/Clr4, which depends on binding trimethyl H3K9 tails via the CD[23,33,53].

For Clr4, the conversion from H3K9me0 to me1 and H3K9me1 to me2 is 10X faster than the conversion from H3K9me2 to me3[23]. This slow step requires significant residence time on the nucleosome and is thus highly sensitive to factors promoting or antagonizing Clr4 substrate access, as well as nucleosome density[54]. Clr4 and Swi6 both make extensive contacts with nucleosomal DNA and the octamer core[17,24]. unpSwi6 and Clr4 affinity to H3K9me0 nucleosomes are very similar (1.8μM and 2.3μM for Clr4[23] and Swi6, respectively), but nuclear Swi6 concentration (2-4 μM) is likely higher than the Clr4 concentration[55]. Thus, unpSwi6 would compete and displace Clr4 from its substrate. However, pSwi6's affinity for the H3K9me0 nucleosome (28μM) is in a regime that is well above its predicted *in vivo* concentration. Any residual competition between pSwi6 and Clr4 would be mitigated by this lower affinity and the

likely higher affinity of the Clr4 complex to its *in vivo* nucleosome substrate, driven by additional chromatin modfications[56].

This lowered pSwi6 nucleosome affinity likely relieves the trimethylation inhibition we observe for unpSwi6 (**Figure 2.7**). Therefore, we propose that a major outcome of Swi6 phosphorylation is to clear nucleosome surfaces for Clr4 to access its substrate (**Figure 2.7G**). We note, that instead of starting with H3K9me0 nucleosomes, we examined the conversion of H3K9me2 to me3. pSwi6 may have increased affinity to those H3K9me2 than H3K9me0 substrates[41]. However, it has been shown that Swi6 isolated from *S. pombe* cells, which is mostly phosphorylated (**Figure 2.7A**), has a significant preference for H3K9me3 over H3K9me2[33]. This lower H3K9me2 preference may still help pSwi6 distinguish between binding H3K9me2 versus me3 chromatin *in vivo*, and not just H3K9me0 versus H3K9me3.

Our *in vivo* data (**Figures 2.1- 2.5, 2.8**) reveals several serines in Swi6 contribute to spreading, but S18 and S24 have a dominant effect. The contribution of other serines is highlighted by 1. A change in nucleosome affinity in pSwi6$^{S18/24A}$ that is 3-4X less than for unpSwi6 (**Figure 2.7F and Table 1**), and, 2. The additional phenotype of *swi6*$^{S18\text{-}220A}$ in gene silencing compared to *swi6*$^{S18/24A}$ (**Figure 2.1**, **Figure 2.2**). Still, why might these two residues, when mutated, have a strong impact on heterochromatin spreading? It is possible that phosphorylation of S18 and S24 plays a disproportional role versus other residues in shifting the Swi6 from the closed to the open state. Alternatively, it is possible that *in vivo*, phosphorylation at S18 and S24 are involved in the recruitment of H3K9me3-promoting factors, including Clr3, and also other factors like Abo1[34,57,58]. Prior work [27] has shown that Clr3 recruitment to heterochromatin is somewhat compromised in *swi6*$^{S18\text{-}117A}$. While this loss of Clr3 may be a consequence of compromised heterochromatin in *swi6*$^{S18\text{-}117A}$, it cannot be excluded that phosphorylation at S18 and S24 is necessary to help recruit Clr3. This would provide another mechanism for Swi6 to support trimethylation spreading by Clr4. Whether this is the case requires further investigation.

Together, we believe that our work resolves a critical problem in heterochromatin biology, which is how “writers” and “readers” promote heterochromatin spreading if they compete for the same substrate surfaces. Phosphorylation of Swi6 tunes the partitioning of Swi6 between unmethylated and methylated nucleosomes *in vivo,* such that Clr4 unmethylated substrates remain largely unbound. Whether this phosphorylation is regulated temporally, at different stages of heterochromatin formation, or spatially, at nucleation versus spreading sites, remains to be investigated.

2.4 Methods

Strain construction

To construct wild-type *swi6* and *swi6* phosphoserine mutants, the swi6 open reading frame (ORF) was first deleted by integrating a *ura4* gene cassette in the MAT HSS background. A plasmid, pRS316, was constructed containing 5' homology-*swi6* promoter-*swi6 (or swi6* S-A mutant*)*- 3' UTR-*kan*-3' genome homology and linearized by PmeI double digest to replace the *ura4* cassette by genomic integration via homologous recombination. After transformation, cells were plated on YES agar for 24 hours before replica plating on G418 selection plates. Isolates were verified by genomic PCR. For Swi6-GFP fusions in the Sad1-mKO2 background, *swi6* wild-type and *swi6* S-A mutant strains were first crossed with the *sad1::mkO2* strain to remove the MAT HSS. Next, *swi6* and *swi6* S-A mutant ORFs were C-terminally fused to SF-GFP followed by a hygromycin resistance marker by CRISPR/Cas9 editing as previously described[59]. Modifications were confirmed by gDNA extraction and PCR amplification of the 5' *swi6* to 3' genome region downstream from the hygromycin marker.

Western blot

Proteins were separated on a 15% SDS-Page gel and transferred to a PVDF membrane (Millipore) for 90 minutes at 100V and 4°C. Membranes were blocked overnight in 1:1 1X PBS: Intercept PBS Blocking Buffer (LiCor). Next, membranes were incubated with either polyclonal anti-Swi6 antibody[25] or anti-pSwi6 antibody (Rockland Immunochemicals, this study) diluted 1:1000 in 1:1 1X PBS, 0.2% Tween-20 (PBS-T): Intercept PBS Blocking Buffer overnight at 4°C on a nutator. Anti-α-tubulin antibody was diluted 1:2000 and used as loading control. Membranes were washed twice with PBS-T for 10 minutes followed by two washes for 5 minutes before incubation with secondary antibodies. Secondary fluorescent antibodies were diluted either 1:10000 (anti-rabbit, 680 nm, Cell Signaling Technology 5366P, lot # 14) or 1:5000

(anti-mouse, 800 nm, Li-Cor, D10603-05) and were incubated with the membranes for 45 minutes at RT. Finally, membranes were washed 3 times with PBS-T for 10 minutes and once with PBS for 10 minutes before imaging on a LiCor Odyssey CLx imager.

HSS Flow cytometry

Strains were struck out of a -80°C freezer onto YES plates. Recovered cells were grown in 200 μL of YES media in a 96-well plate overnight to saturation at 32°C. The next morning, cells were diluted 1:25 in YES media into mid-log phase and analyzed by flow cytometry on an LSR Fortessa X50 (BD Biosciences). Fluorescence compensation, data analysis, and plotting in R were performed as described in Greenstein *et al.* 2022[33].

Chromatin immunoprecipitation followed by sequencing (ChIP -seq) sample collection and library preparation

Cells were grown in YES media overnight to saturation (32°C, 225RPM shaking). The following morning cells were diluted to OD 0.03, grown to OD 1, and 300x10^6 were fixed and frozen at -80°C. Cells were processed for ChIP as described in Canzio *et al.* 2011 with the following modifications: Three technical replicates were processed for ChIP-seq. After lysis, cells were bead beat 10 rounds for 1 minute each round with 0.5 mm Zirconia/Silica beads (Cat No. 11079105z). Tubes were chilled on ice for 2 minutes between rounds. Lysates were then spun down to isolate chromatin. The chromatin pellet was resuspended in 1.5 mL lysis buffer, moved to a 15 mL Diagenode Bioruptor tube (Cat. No. C01020031) and sonicated with a Diagenode Bioruptor Pico sonicator for a total of 35 cycles, 30 seconds on/ 30 seconds off, in the presence of sonication beads (Diagenode, Cat. No. C03070001). Every 10 cycles tubes were vortexed. Chromatin lysate was spun down for 30 minutes at 14000 RPM and 4°C. The lysate volume was brought up to 900 µL. 45 µL was taken out to check shearing of the DNA. 40

µL was taken out for input and kept at RT until the reverse crosslinking step. The remaining ~800 µL was divided into 2 tubes to incubate with either 2 µL anti-H3K9me2 (Abcam 1120, Lot No. 1009758-6) or 1 µg anti-H3K9me3 (Diagenode, Cat. No. C15500003 Lot No. 003) overnight on a tube rotator at 4°C. The next morning, Protein A Dynabeads (Invitrogen, LOT 01102248) and M280 Streptavidin beads (Invitrogen, LOT 2692541) were washed twice with Lysis Buffer without protease inhibitors. 20 µL Protein A Dynabeads beads were added to each anti-H3K9me2 sample, and 30 µL M-280 Streptavidin beads were added to each anti-H3K9me3 sample. Beads were incubated with samples for 3 hours on a tube rotator at 4°C, and then washed with 700 µL cold buffers at RT on a tube rotator in the following order: 2X Lysis Buffer for 5 minutes, 2X High Salt Buffer for 5 minutes, 1X Wash Buffer for 5 minutes, and 1X TE (buffer recipes as in[60]). Samples were incubated with 100 µL elution buffer (50 mM Tris pH 8.0, 10 mM EDTA, 1% SDS) for 20 minutes at 70°C in a ThermoMixer F1.5 (Eppendorf). Input samples were brought up to 100 µL in TE with a final concentration of 1% SDS. Input and eluted samples were then incubated overnight in a 65°C water bath with 2.5 µL 2.5 mg/mL Proteinase K (Sigma Aldrich, Lot 58780500) for reverse crosslinking. Samples were purified with a PCR clean-up kit (Machery-Nagel) and eluted in 100 µL 10 mM Tris pH 8.0. The quality and size of the DNA were assessed by 4200 TapeStation instrument (Agilent). Next, libraries were prepared using Index Primer Set 1 (NEBNext Multiplex Oligos for Illumina, E7335L, Lot 10172541), Ultra II FS DNA Library Prep Kit for Illumina (E7805L, Lot 10202083). The manufacturer's protocol, "Protocol for FS DNA Library Prep Kit (E7805, E6177) with Inputs ≤100 ng (NEB)", was used starting with 200 pg of DNA. PCR-enriched adaptor-ligated DNA was cleaned up using NEBNext sample purification beads (E6178S, Lot 10185312, "1.5. Cleanup of PCR Reaction" in manufacturer's protocol). Individual adaptor-ligated DNA sample concentrations were quantified using a Qubit 4 Fluorometer (Thermo Fisher), and the quality of the DNA was assessed by a 4200 TapeStation instrument (Agilent). Libraries were pooled to

equimolar quantities and sequenced using a NextSeq 2000 P2 (400 million clusters) (Chan Zuckerberg Biohub San Francisco) (40bp read length, paired-end).

ChIP-seq data analysis

Sequencing adaptors were trimmed from raw sequencing reads using Trimmomatic v0.39. The S. pombe genome was downloaded from NCBI under Genome Assembly ASM294v2. The MAT locus of chromosome II was edited to our custom HSS MAT locus, and the genome was indexed using the bowtie2-build function of Bowtie2 v2.5.1[61]. Trimmed sequencing reads were aligned to the genome using Bowtie2 v2.5.1 with flags [--local --very-sensitive-local --no-unal --no-mixed --no-discordant --phred33 -I 10 -X 700][62]. Next, the resulting SAM files were converted to BAM files using SAMtools v1.18[63] view function: -S -b ${base}.sam > ${base}.bam. The resulting BAM files were further processed by removing low-quality alignments, PCR duplicates, and multimappers, and retain properly aligned paired-end reads using SAMtools view with the following flags: -bh -F 3844 -f 3 -q 10 -@ 4. The processed BAM files were then sorted and indexed (SAMtools). Sorted, indexed BAM files were converted to bigWig coverage tracks using deepTools v3.5.4[64]: bamCoverage: -b "$bam_file" -o "$filename_without_extension.bw" --binSize 10 --normalizeUsing CPM --extendReads --exactScaling --samFlagInclude 64 --effectiveGenomeSize 13000000. BigWig files normalized to input were generated using the bigwigCompare tool (deepTools). Normalized bigWig files were loaded into R v4.3.0 using rtracklayer v1.60.1[65] and processed for visualization as in Greenstein *et al.* 2022 with modifications. The Gviz v1.44.2 (Bioconductor) DataTrack function was used to create a visualization track of ChIP-seq signal in bigWig files for each genotype[66]. The Bioconductor GenomicRanges package was used to create a GRanges object to store custom genomic coordinates defined by a BEDfile[67]. Genomic annotations for signal tracks were created using the AnnotationTrack (Gviz) function. The GenomeAxisTrack (Gviz) function generated a visual reference (in megabases) to display the position of genomic annotations and

signal tracks. Finally, the plotTracks (Gviz) function was used to plot the DataTrack, AnnotationTrack, and GenomeAxisTrack objects for visualization.

Swi6-GFP live cell imaging

Swi6-GFP/Sad1-mKO2 strains were struck out onto fresh YES 225 agar plates and incubated at 32°C for 3-5 days. Colonies were inoculated into liquid YES 225 medium (#2011, Sunrise Science Production) and grown in an incubator shaker at 30°C, 250 rpm to an OD of 0.2 -0.6. Cells were placed onto 2% agarose (#16500500, Invitrogen) pads in YES 225, covered with a coverslip (#2850-22, thickness 1 ½, Corning), and sealed with VALAP for imaging. Cells were imaged on a Ti-Eclipse inverted microscope (Nikon Instruments) with a spinning-disk confocal system (Yokogawa CSU-10) and a Borealis illumination system that includes 488nm and 541nm laser illumination and emission filters 525±25nm and 600±25nm respectively, 60X (NA: 1.4) objectives, and an EM-CCD camera (Hamamatsu, C9100-13). These components were controlled with μManager v. 1.41[68,69]. The temperature of the sample was maintained at 30°C by a black panel cage incubation system (#748–3040, OkoLab). The middle plane of cells was first imaged in brightfield and then two Z-stacks with a step size of 0.5μm were acquired in spinning-disk confocal mode with laser illumination 488nm and 541nm (total of 9 imaging planes per channel). The exposure, laser power, and EM gain for the Z-stacks were respectively 50ms / 1% / 800, and 200ms / 5% / 800. Between 9 and 12 fields of view were acquired per strain.

Image analysis

For each field of view, nuclei were manually cropped using Fiji. Cells containing multiple Sad1-mK02 foci were discarded from this analysis. For each selected nucleus TrackMate was used to determine the coordinates in space (X, Y, Z) of Sad1 and every Swi6 focus and their fluorescence intensity[70,71]. Using a custom script on Jupiter Notebook in Python we then automatically counted the number of Swi6 foci detected by TrackMate for each nucleus.

Additionally, we automated the calculation of the distance between Swi6 foci and the spindle pole body by measuring the distance from each Swi6 focus to Sad1 within a given nucleus. For Swi6 intensity measurements, a region of interest (ROI) outside of each nucleus was automatically selected to measure the background intensity. This background intensity was then used to correct Swi6 fluorescence signal by subtracting the average intensity of this ROI for a given analyzed nucleus. Finally, we used a one-way ANOVA statistical test on Swi6 intensity signal to determine differences between mutants.

Protein cloning and purification

Wildtype *swi6* open reading frame was cloned by ligation-independent cloning into vector 14B (QB3 Berkeley Macrolab expression vectors). Vector 14B encodes an N-terminal 6xHis tag followed by a TEV cleavage sequence. Wildtype Swi6 was expressed in BL21-gold (DE3) competent cells. To produce $Swi6^{S18/24A}$, a gene block containing S18A/S24A Swi6 was cloned into vector 14B using Gibson assembly. To isolate pSwi6 and $pSwi6^{S18/S24A}$, the respective vectors were co-expressed with the catalytic subunits of Caesin Kinase II in pRSFDuet. All three proteins were grown, harvested, and purified using a protocol adapted from [10] and modified as follows: Cells were grown at 37°C until OD600 0.5-0.6 and induced with a final concentration of 0.4mM Isopropyl-β-D-thiogalactopyranoside. Induced cells were grown at 18°C overnight. Harvested cells were resuspended in lysis buffer containing 1X PBS buffer pH 7.3, 300 mM NaCl, 10% glycerol, 0.1% Igepal CA-630, 7.5 mM Imidazole, 1 mM Beta-Mercaptoethanol (βME), with protease inhibitors. Resuspended cells were sonicated 2 seconds on /2 seconds off at 40% output power for three 5-minute cycles. The lysate was centrifuged at 25,000xg for 25 minutes, and the supernatant was collected. Nickel NTA resin was equilibrated with lysis buffer. The supernatant and resin were incubated for 1-2 hours and washed 3 times with 40 ml of lysis buffer each time before the protein was eluted with 25 mM HEPES pH 7.5, 100 mM KCl, 10% glycerol, 400 mM Imidazole, and 1 mM βME. The eluted protein was then

dialyzed in TEV cleavage buffer containing 25 mM HEPES pH 7.5, 100 mM KCl, and 1 mM βME and 6 mg TEV protease. The following morning 3-6 mg of TEV protease was spiked in for about 1 hour to ensure full cleavage. Nickel NTA resin was equilibrated with TEV cleavage buffer and the his-tagged TEV was captured by the resin while Swi6 protein was isolated by gravity flow. Cleaved protein was concentrated using a 10kDa MWCO concentrator and applied to a Superdex 200 Increase 10/300 GL size exclusion column equilibrated in storage buffer containing 25 mM HEPES pH 7.5, 100 mM KCl, 10% glycerol, and 10 mM βME. Protein was concentrated, flash-frozen in N_2 (liq), and stored at -80°C. Protein concentration was quantified against a BSA standard curve on an SDS page gel and sypro red stain.

EDC/NHS crosslinking

unpSwi6 or pSwi6 was purified as described above. However, the storage buffer was 25 mM HEPES pH 7.5 and 100 mM KCl for SEC-MALS. Protein, either 100 µM Swi6 or pSwi6, was incubated with 2 mM EDC and 5 mM NHS in a total volume of 95 µL for 2 hours. The reaction was quenched with a final concentration of 20 mM hydroxylamine.

Size-exclusion Chromatography coupled with Multi-Angle Light Scattering (SEC-MALS)

Crosslinked and uncrosslinked Swi6 and pSwi6 were filtered with 0.2 µm spin columns (Pall Corporation, Ref. ODM02C34). For SEC, uncrosslinked and crosslinked proteins were injected onto a KW-804 silica gel chromatography column (Shodex) in a volume of 50 µL at 100 µM. The column was run using an ÄKTA pure FPLC (GE Healthcare Life Sciences) and equilibrated with SEC-MALS storage buffer at a flow rate of 0.4 mL/min and temperature of 8°C. The SEC column was connected in-line to a DAWN HELEOS II (Wyatt Technology) 18-angle light scattering instrument and an Optilab T-rEX differential refractive index detector (Wyatt

Technology). Data was analyzed using ASTRA software (version 7.1.4.8, Wyatt Technology) and graphed using GraphPad Prism software (version 9.5.1).

Fluorescence Polarization

Fluorescence Polarization binding measurements were conducted as described in Canzio *et al.* 2013 and modified as follows:

Peptide reaction buffer was 50 mM HEPES pH 7.5, 100 mM KCl, 10% glycerol, 0.01% NP-40, and 2 mM βME. Fluoresceinated $H3_{1-20}$ K9me0 or $H3_{1-20}$ K9me3 peptide concentration was fixed at 100 nM while Swi6, pSwi6, or $pSwi6^{S18/24A}$ protein concentration varied from 0-200 μM. Mononuclesome reaction buffer was 20 mM HEPES pH 7.5, 80 mM KCl, 4 mM Tris, 0.2 mM EDTA, 10% glycerol, 0.01% NP-40, 2 mM βME. H3K9me0 and $H3K_C9me3$ mononucleosomes were reconstituted with fluorescein-labeled 601 DNA as described[12]. Nucleosome concentration was fixed at 25 nM while Swi6, pSwi6, or $pSwi6^{S18/24A}$ protein concentrations varied from 0-200 μM. Both peptide and mononucleosome reaction volumes were 10 μL and measured in a Corning 384 low-volume, flat bottom plates (product number 3820, LOT 23319016). Fluorescence polarization was recorded using a Cytation 5 microplate reader (Biotek, λ_{ex}= 485/20nm, λ_{em}= 528/20nm) and Gen5 software (Biotek, version 3.09.07). Data was analyzed and fit to a K_d equation using GraphPad Prism.

Single turnover kinetics

Clr4 protein was purified exactly as described[23]. H3K9me2 nucleosomes were purchased from Epicypher (#16-0324), and pSwi6 and unpSwi6 were purified as above. Single turnover reactions were carried out as follows: 5 μM Clr4 was preincubated 5 minutes with 1 mM final S-adenosyl-methionine (liquid SAM, 3 2mM, NEB #B9003S), and varying concentrations of pSwi6 or unP Swi6, at 25°C to reach equilibrium. 5μM Clr4 was chosen as the

minimal Clr4 concentration to yield robust H3K9me3 signal under Single Turnover conditions. The reaction was started with the addition of H3K9me2 nucleosomes to 500nM final. Timepoints were stopped by boiling with SDS-Laemmli buffer. Samples were separated on 18% SDS-PAGE gel and probed for the presence of H3K9me3 (polyclonal, Active Motif #39161. lot 22355218-11) and H4 (Active Motif #39269 lot 31519002) as a loading control. Signals were quantified on a Li-Cor imager by using a dilution of H3K9me3 nucleosomes (Epicypher, #16-0315), establishing standard curves for H4 and H3K9me3. Rates were fit to a single exponential rise in GraphPad Prism software exactly as published[23].

Phosphatase treatments

1500 ng of Swi6, pSwi6, and pSwi6$^{S18/24A}$ were incubated for 20 minutes at 37°C with 50 U of Calf Intestinal Phosphatase (QuickCIP, NEB, M0525S) in 100 mM NaCl, 50 mM Tris-HCl, 10 mM $MgCl_2$, 1 mM dithiothreitol, pH 7.9. Reactions were stopped by boiling in SDS-Laemmli buffer. For reactions with inactivated CIP, 200U CIP was pre-incubated for 20 minutes at 80°C. 75 ng of Swi6, pSwi6, and pSwi6$^{S18/24A}$ that was either mock-treated, treated with active or inactivated CIP was separated on either a 15% SDS-PAGE gel or a SuperSep Phos-Tag gel (Fujifilm, 15.5%, 17 well, 100x100x6.6mm, Lot PAR5302). The Phos-Tag gel was washed with western transfer buffer with 10 mM EDTA to remove Zn^{2+} ions and then blotted and probed for Swi6 with Swi6 polyclonal antibody as above.

Mass Spectrometry

In-solution Trypsin/Lys C digested peptides were analyzed by online capillary nanoLC-MS/MS using several different methods. High resolution 1 dimensional LCMS was performed using a 25 cm reversed-phase column fabricated in-house (75 µm inner diameter, packed with ReproSil-Gold C18-1.9 µm resin (Dr. Maisch GmbH)) that was equipped with a laser-pulled nanoelectrospray emitter tip. Peptides were eluted at a flow rate of 300 nL/min using a linear

gradient of 2–40% buffer B in 140 min (buffer A: 0.02% HFBA and 5% acetonitrile in water; buffer B: 0.02% HFBA and 80% acetonitrile in water) in a Thermo Fisher Easy-nLC1200 nanoLC system. Peptides were ionized using a FLEX ion source (Thermo Fisher) using electrospray ionization into a Fusion Lumos Tribrid Orbitrap Mass Spectrometer (Thermo Fisher Scientific). Data was acquired in orbi-trap mode. Instrument method parameters were as follows: MS1 resolution, 120,000 at 200 m/z; scan range, 350−1600 m/z. The top 20 most abundant ions were subjected to higher-energy collisional dissociation (HCD) or electron transfer dissociation (ETD) with a normalized collision energy of 35%, activation q 0.25, and precursor isolation width 2 m/z. Dynamic exclusion was enabled with a repeat count of 1, a repeat duration of 30 seconds, and an exclusion duration of 20 seconds.

Low-resolution, 1-dimensional LCMS was performed using a nano-LC column packed in a 100-μm inner diameter glass capillary with an integrated pulled emitter tip. The column consisted of 10 cm of ReproSil-Gold C18-3 μm resin (Dr. Maisch GmbH)). The column was loaded and conditioned using a pressure bomb. The column was then coupled to an electrospray ionization source mounted on a Thermo-Fisher LTQ XL linear ion trap mass spectrometer. An Agilent 1200 HPLC equipped with a split line so as to deliver a flow rate of 1 ul/min was used for chromatography. Peptides were eluted with a 90-minute gradient from 100% buffer A to 60% buffer B. Buffer A was 5% acetonitrile/0.02% heptafluorobutyric acid (HBFA); buffer B was 80% acetonitrile/0.02% HBFA. Collision-induced dissociation spectra were collected for each m/z. Multidimensional protein identification technique (MudPIT) was performed as described[72,73]. Briefly, a 2D nano-LC column was packed in a 100-μm inner diameter glass capillary with an integrated pulled emitter tip. The column consisted of 10 cm of ReproSil-Gold C18-3 μm resin (Dr. Maisch GmbH)) and 4 cm strong cation exchange resin (Partisphere, Hi Chrom). The column was loaded and conditioned using a pressure bomb. The column was then coupled to an electrospray ionization source mounted on a Thermo-Fisher LTQ XL linear ion trap mass spectrometer. An Agilent 1200 HPLC equipped with a split line so as to deliver a flow rate of 1

ul/min was used for chromatography. Peptides were eluted using a 4-step gradient with 4 buffers. Buffer (A) 5% acetonitrile, 0.02% heptafluorobutyric acid (HFBA), buffer (B) 80% acetonitrile, 0.02% HFBA, buffer (C) 250mM NH4AcOH, 0.02% HFBA, (D) 500mM NH4AcOH, 0.02% HFBA. Step 1: 0-80% (B) in 70 min, step 2: 0-50% (C) in 5 min and 0- 45% (B) in 100 min, step 3: 0-100% (C) in 5 min and 0- 45% (B) in 100 min, step 4 0-100% (D) in 5 min and 0-45% (B) in 160 min. Collision-induced dissociation (CID) spectra were collected for each m/z. Data analysis: RAW files were analyzed using PEAKS (Bioinformatics Solution Inc) with the following parameters: semi-specific cleavage specificity at the C-terminal site of R and K, allowing for 5 missed cleavages, precursor mass tolerance of 15 ppm (3 Da for low-resolution LCMS), and fragment ion mass tolerance of 0.5 Daltons. Methionine oxidation and phosphorylation of serine, threonine, and tyrosine were set as variable modifications and Cysteine carbamidomethylation was set as a fixed modification. Peptide hits were filtered using a 1% false discovery rate (FDR). Phosphorylation occupancy ratio for amino acids was determined by summing the count of unphosphorylated and phosphorylated amino acids detected in the experiment. We only considered phospho-peptides detected more than once and at least 2% minimal ion intensity.

Estimate of in vivo nucleosome fractions bound

In vitro binding isotherms for nucleosomes (N) can be fit simply via $fraction\ Nbound = \frac{[Swi6]}{[Swi6]+Kd}$. However, this assumes first that [N] << [Swi6] and << K_d, such that [Swi6] total ≈ [Swi6] free. In the nucleus, these assumptions do not hold. However, a quadratic equation[46] can be used to estimate N bound, accounting for bound Swi6. In this case,

$frNbound = \frac{[N]total+[Swi6]total+Kd-\sqrt{([N]total+[Swi6]total+Kd)^2-4*[N]total*[Swi6]total}}{2*[N]total}$. To estimate the fraction of unmethylated nucleosomes bound by pSwi6 or unpSwi6, we used K_ds from Figure 2.7F, total Swi6 concentrations of 2.1-4.6μM, and total nucleosome contraction estimate of ~10μM.

Table 2: Yeast strains used in this study.
List of *S. pombe* strains with individual identifier, genotype, the figure the strain is associated with, and source.

Identifier	Genotype	Figure; experiment	Source
PAS210	h+, *sad1*:mKO2:NATMX	Fig. 2.5G, H; Fig. 2.8	Al-Sady *et al*. 2016
PAS807	h90, cenH:: ade6p:SF-GFP (Kint2); mat3m(EcoRV):: ade6p:mKO2; ade6p:3xE2C:hygMX at Locus2; ΔREIII::REIII(Δs1, Δs2), *swi6::ura4*	Fig. 2.1C, D; Fig. 2.3B; Fig. 2.4 A-C	This study
PAS814	h90, cenH:: ade6p:SF-GFP (Kint2); mat3m(EcoRV):: ade6p:mKO2; ade6p:3xE2C:hygMX at Locus2; ΔREIII::REIII(Δs1, Δs2), *swi6*:KANMX	Fig. 2.1C, E; Fig. 2.3B-D; Fig. 2.4A-C	This study
PAS851,858, 859, 860 (isolates)	h90, cenH:: ade6p:SF-GFP (Kint2); mat3m(EcoRV):: ade6p:mKO2; ade6p:3xE2C:hygMX at Locus2; ΔREIII::REIII(Δs1, Δs2), *swi6S18/24A*:KANMX	Fig. 2.1C, G; Fig. 2.2A-C; Fig. 2.3B-D; Fig. 2.4A-C	This study
PAS852, 861,862, 863 isolates)	h90, cenH:: ade6p:SF-GFP (Kint2); mat3m(EcoRV):: ade6p:mKO2; ade6p:3xE2C:hygMX at Locus2; ΔREIII::REIII(Δs1, Δs2), *swi6S46/52,117-220A*:KANMX	Fig. 2.1C, H; Fig. 2.2D-F	This study
PAS853, 864, 865, 866 (isolates)	h90, cenH:: ade6p:SF-GFP (Kint2); mat3m(EcoRV):: ade6p:mKO2; ade6p:3xE2C:hygMX at Locus2; ΔREIII::REIII(Δs1, Δs2), *swi6S46/52*:KANMX	Fig. 2.1C, F	This study
PAS854	h90, cenH:: ade6p:SF-GFP (Kint2); mat3m(EcoRV):: ade6p:mKO2; ade6p:3xE2C:hygMX at Locus2; ΔREIII::REIII(Δs1, Δs2), *swi6S18/24,117-220A*:KANMX	Fig. 2.1C, I	This study
PAS909	*sad1*:mKO2:NATMX; *swi6S46/52*:SF-GFP:HYGMX	Fig. 2.8B-F	This study
PAS910,911	*sad1*:mKO2:NATMX; *swi6S18/24,117-220A*:SF-GFP:HYGMX	Fig. 2.5 G, H; Fig. 2.8 C-F	This study
PAS913	*sad1*:mKO2:NATMX; *swi6*:SF-GFP:HYGMX	Fig 2.5 G, H; Fig. 2.8C-F	This study
PAS919	*sad1*:mKO2:NATMX; *swi6S18/24*:SF-GFP:HYGMX	Fig. 2.5G, H; Fig. 2.8C-F	This study
PAS922	*sad1*:mKO2:NATMX; *swi6S46/52,117-220A*:SF-GFP:HYGMX	Fig. 2.5G, H; Fig. 2.8C-F	This study

3. References

1. Grewal, S. I. S. The molecular basis of heterochromatin assembly and epigenetic inheritance. *Mol. Cell* **83**, 1767–1785 (2023).
2. Hamali, B., Amine, A. A. A. & Al-Sady, B. Regulation of the heterochromatin spreading reaction by trans-acting factors. *Open Biol.* **13**, 230271 (2023).
3. Elgin, S. C. & Reuter, G. Position-effect variegation, heterochromatin formation, and gene silencing in Drosophila. *Cold Spring Harb Perspect Biol* **5**, a017780 (2013).
4. Zhang, K., Mosch, K., Fischle, W. & Grewal, S. I. S. Roles of the Clr4 methyltransferase complex in nucleation, spreading and maintenance of heterochromatin. *Nat Struct Mol Biol* **15**, 381–8 (2008).
5. Muller, M. M., Fierz, B., Bittova, L., Liszczak, G. & Muir, T. W. A two-state activation mechanism controls the histone methyltransferase Suv39h1. *Nat Chem Biol* **12**, 188–93 (2016).
6. Noma, K. *et al.* RITS acts in cis to promote RNA interference-mediated transcriptional and post-transcriptional silencing. *Nat Genet* **36**, 1174–80 (2004).
7. Hall, I. M. *et al.* Establishment and maintenance of a heterochromatin domain. *Science* **297**, 2232–2237 (2002).
8. Jacobs, S. A. & Khorasanizadeh, S. Structure of HP1 chromodomain bound to a lysine 9-methylated histone H3 tail. *Science* **295**, 2080–3 (2002).
9. Haldar, S., Saini, A., Nanda, J. S., Saini, S. & Singh, J. Role of Swi6/HP1 self-association-mediated recruitment of Clr4/Suv39 in establishment and maintenance of heterochromatin in fission yeast. *J Biol Chem* **286**, 9308–20 (2011).
10. Jenuwein, T. & Allis, C. D. Translating the histone code. *Science* **293**, 1074–80 (2001).

11. Aagaard, L., Schmid, M., Warburton, P. & Jenuwein, T. Mitotic phosphorylation of SUV39H1, a novel component of active centromeres, coincides with transient accumulation at mammalian centromeres. *J. Cell Sci.* **113 (Pt 5)**, 817–829 (2000).
12. Canzio, D. *et al.* Chromodomain-mediated oligomerization of HP1 suggests a nucleosome-bridging mechanism for heterochromatin assembly. *Mol. Cell* **41**, 67–81 (2011).
13. Larson, A. G. *et al.* Liquid droplet formation by HP1α suggests a role for phase separation in heterochromatin. *Nature* **547**, 236–240 (2017).
14. Sanulli, S. & J Narlikar, G. Liquid-like interactions in heterochromatin: Implications for mechanism and regulation. *Curr. Opin. Cell Biol.* **64**, 90–96 (2020).
15. Keenen, M. M. *et al.* HP1 proteins compact DNA into mechanically and positionally stable phase separated domains. *eLife* **10**, (2021).
16. Strom, A. R. *et al.* Phase separation drives heterochromatin domain formation. *Nature* **547**, 241–245 (2017).
17. Sanulli, S. *et al.* HP1 reshapes nucleosome core to promote phase separation of heterochromatin. *Nature* **575**, 390–394 (2019).
18. Holla, S. *et al.* Positioning Heterochromatin at the Nuclear Periphery Suppresses Histone Turnover to Promote Epigenetic Inheritance. *Cell* **180**, 150-164.e15 (2020).
19. Fischer, T. *et al.* Diverse roles of HP1 proteins in heterochromatin assembly and functions in fission yeast. *Proc Natl Acad Sci USA* **106**, 8998–9003 (2009).
20. Verschure, P. J. *et al.* In vivo HP1 targeting causes large-scale chromatin condensation and enhanced histone lysine methylation. *Mol Cell Biol* **25**, 4552–64 (2005).
21. Keller, C. *et al.* HP1(Swi6) Mediates the Recognition and Destruction of Heterochromatic RNA Transcripts. *Mol. Cell* **47**, 215–27 (2012).
22. Motamedi, M. R. *et al.* HP1 proteins form distinct complexes and mediate heterochromatic gene silencing by nonoverlapping mechanisms. *Mol. Cell* **32**, 778–90 (2008).

23. Al-Sady, B., Madhani, H. D. & Narlikar, G. J. Division of labor between the chromodomains of HP1 and Suv39 methylase enables coordination of heterochromatin spread. *Mol. Cell* **51**, 80–91 (2013).

24. Akoury, E. *et al.* Disordered region of H3K9 methyltransferase Clr4 binds the nucleosome and contributes to its activity. *Nucleic Acids Res* **47**, 6726–6736 (2019).

25. Canzio, D. *et al.* A conformational switch in HP1 releases auto-inhibition to drive heterochromatin assembly. *Nature* **496**, 377–81 (2013).

26. Shirai, A. *et al.* Impact of nucleic acid and methylated H3K9 binding activities of Suv39h1 on its heterochromatin assembly. *Elife* **6**, (2017).

27. Shimada, A. *et al.* Phosphorylation of Swi6/HP1 regulates transcriptional gene silencing at heterochromatin. *Genes Dev* **23**, 18–23 (2009).

28. Eissenberg, J. C., Ge, Y. W. & Hartnett, T. Increased phosphorylation of HP1, a heterochromatin-associated protein of Drosophila, is correlated with heterochromatin assembly. *J. Biol. Chem.* **269**, 21315–21321 (1994).

29. LeRoy, G. *et al.* Heterochromatin Protein 1 Is Extensively Decorated with Histone Code-like Post-translational Modifications*. *Mol. Cell. Proteomics* **8**, 2432–2442 (2009).

30. Nishibuchi, G. *et al.* N-terminal phosphorylation of HP1alpha increases its nucleosome-binding specificity. *Nucleic Acids Res* **42**, 12498–511 (2014).

31. Greenstein, R. A. *et al.* Local chromatin context regulates the genetic requirements of the heterochromatin spreading reaction. *PLoS Genet.* **18**, e1010201 (2022).

32. Greenstein, R. A. *et al.* Noncoding RNA-nucleated heterochromatin spreading is intrinsically labile and requires accessory elements for epigenetic stability. *eLife* **7**, e32948 (2018).

33. Jih, G. *et al.* Unique roles for histone H3K9me states in RNAi and heritable silencing of transcription. *Nature* (2017) doi:10.1038/nature23267.

34. Yamada, T., Fischle, W., Sugiyama, T., Allis, C. D. & Grewal, S. I. S. The nucleation and maintenance of heterochromatin by a histone deacetylase in fission yeast. *Mol. Cell* **20**, 173–85 (2005).

35. Cheutin, T., Gorski, S. A., May, K. M., Singh, P. B. & Misteli, T. In Vivo Dynamics of Swi6 in Yeast: Evidence for a Stochastic Model of Heterochromatin. *Mol Cell Biol* **24**, 3157–3167 (2004).

36. Hiragami-Hamada, K. *et al.* N-terminal phosphorylation of HP1{alpha} promotes its chromatin binding. *Mol. Cell. Biol.* **31**, 1186–1200 (2011).

37. Williams, J. F. *et al.* The condensation of HP1-α/Swi6 imparts nuclear stiffness. 2020.07.02.184127 Preprint at https://doi.org/10.1101/2020.07.02.184127 (2023).

38. Biswas, S. *et al.* HP1 oligomerization compensates for low-affinity H3K9me recognition and provides a tunable mechanism for heterochromatin-specific localization. *Sci. Adv.* **8**, eabk0793 (2022).

39. Simon, M. D. *et al.* The site-specific installation of methyl-lysine analogs into recombinant histones. *Cell* **128**, 1003–12 (2007).

40. Carpy, A. *et al.* Absolute proteome and phosphoproteome dynamics during the cell cycle of Schizosaccharomyces pombe (Fission Yeast). *Mol. Cell. Proteomics MCP* **13**, 1925–1936 (2014).

41. Sadaie, M. *et al.* Balance between Distinct HP1 Family Proteins Controls Heterochromatin Assembly in Fission Yeast. *Mol Cell Biol* **28**, 6973–6988 (2008).

42. Lemière, J., Real-Calderon, P., Holt, L. J., Fai, T. G. & Chang, F. Control of nuclear size by osmotic forces in Schizosaccharomyces pombe. *eLife* **11**, e76075 (2022).

43. Neumann, F. R. & Nurse, P. Nuclear size control in fission yeast. *J Cell Biol* **179**, 593–600 (2007).

44. Lantermann, A. B. *et al.* Schizosaccharomyces pombe genome-wide nucleosome mapping reveals positioning mechanisms distinct from those of Saccharomyces cerevisiae. *Nat Struct Mol Biol* **17**, 251-U15 (2010).

45. Godde, J. S. & Widom, J. CHROMATIN STRUCTURE OF SCHIZOSACCHAROMYCES-POMBE - A NUCLEOSOME REPEAT LENGTH THAT IS SHORTER THAN THE CHROMATOSOMAL DNA LENGTH. *J Mol Biol* **226**, 1009–1025 (1992).

46. Jarmoskaite, I., AlSadhan, I., Vaidyanathan, P. P. & Herschlag, D. How to measure and evaluate binding affinities. *eLife* **9**, e57264 (2020).

47. Hou, H. *et al.* Csi1 links centromeres to the nuclear envelope for centromere clustering. *J. Cell Biol.* **199**, 735–744 (2012).

48. Barrales, R. R., Forn, M., Georgescu, P. R., Sarkadi, Z. & Braun, S. Control of heterochromatin localization and silencing by the nuclear membrane protein Lem2. *Genes Dev* **30**, 133–48 (2016).

49. Al-Sady, B., Greenstein, R. A., El-Samad, H. J., Braun, S. & Madhani, H. D. Sensitive and Quantitative Three-Color Protein Imaging in Fission Yeast Using Spectrally Diverse, Recoded Fluorescent Proteins with Experimentally-Characterized In Vivo Maturation Kinetics. *PLoS One* **11**, e0159292 (2016).

50. Zhao, T., Heyduk, T. & Eissenberg, J. C. Phosphorylation site mutations in heterochromatin protein 1 (HP1) reduce or eliminate silencing activity. *J. Biol. Chem.* **276**, 9512–9518 (2001).

51. Zhao, T. & Eissenberg, J. C. Phosphorylation of heterochromatin protein 1 by casein kinase II is required for efficient heterochromatin binding in Drosophila. *J. Biol. Chem.* **274**, 15095–15100 (1999).

52. Nishibuchi, G. *et al.* Mitotic phosphorylation of HP1α regulates its cell cycle-dependent chromatin binding. *J. Biochem. (Tokyo)* **165**, 433–446 (2019).

53. Murawska, M. *et al.* The histone chaperone FACT facilitates heterochromatin spreading by regulating histone turnover and H3K9 methylation states. *Cell Rep.* **37**, 109944 (2021).

54. Cutter DiPiazza, A. R. *et al.* Spreading and epigenetic inheritance of heterochromatin require a critical density of histone H3 lysine 9 tri-methylation. *Proc. Natl. Acad. Sci. U. S. A.* **118**, e2100699118 (2021).

55. Iglesias, N. *et al.* Native Chromatin Proteomics Reveals a Role for Specific Nucleoporins in Heterochromatin Organization and Maintenance. *Mol. Cell* **77**, 51-66.e8 (2020).

56. Stirpe, A. *et al.* SUV39 SET domains mediate crosstalk of heterochromatic histone marks. *eLife* **10**, e62682 (2021).

57. Zofall, M., Sandhu, R., Holla, S., Wheeler, D. & Grewal, S. I. S. Histone deacetylation primes self-propagation of heterochromatin domains to promote epigenetic inheritance. *Nat. Struct. Mol. Biol.* **29**, 898–909 (2022).

58. Dong, W. *et al.* Abo1 is required for the H3K9me2 to H3K9me3 transition in heterochromatin. *Sci. Rep.* **10**, 6055 (2020).

59. Torres-Garcia, S. *et al.* SpEDIT: A fast and efficient CRISPR/Cas9 method for fission yeast. *Wellcome Open Res.* **5**, 274 (2020).

60. Rougemaille, M., Shankar, S., Braun, S., Rowley, M. & Madhani, H. D. Ers1, a rapidly diverging protein essential for RNA interference-dependent heterochromatic silencing in Schizosaccharomyces pombe. *J. Biol. Chem.* **283**, 25770–25773 (2008).

61. Bolger, A. M., Lohse, M. & Usadel, B. Trimmomatic: a flexible trimmer for Illumina sequence data. *Bioinforma. Oxf. Engl.* **30**, 2114–2120 (2014).

62. Langmead, B. & Salzberg, S. L. Fast gapped-read alignment with Bowtie 2. *Nat. Methods* **9**, 357–359 (2012).

63. Li, H. *et al.* The sequence alignment/map format and SAMtools. *Bioinformatics* **25**, 2078–2079 (2009).

64. Ramírez, F., Dündar, F., Diehl, S., Grüning, B. A. & Manke, T. DeepTools: A flexible platform for exploring deep-sequencing data. *Nucleic Acids Res* **42**, W187–W191 (2014).

65. Lawrence, M., Gentleman, R. & Carey, V. rtracklayer: an R package for interfacing with genome browsers. *Bioinforma. Oxf. Engl.* **25**, 1841–1842 (2009).

66. Hahne, F. & Ivanek, R. Visualizing Genomic Data Using Gviz and Bioconductor. *Methods Mol. Biol. Clifton NJ* **1418**, 335–351 (2016).

67. GenomicRanges. *Bioconductor* http://bioconductor.org/packages/GenomicRanges/.

68. Edelstein, A. D. *et al.* Advanced methods of microscope control using μManager software. *J. Biol. Methods* **1**, e10 (2014).

69. Edelstein, A., Amodaj, N., Hoover, K., Vale, R. & Stuurman, N. Computer control of microscopes using μManager. *Curr. Protoc. Mol. Biol.* **Chapter 14**, Unit14.20 (2010).

70. Ershov, D. *et al.* TrackMate 7: integrating state-of-the-art segmentation algorithms into tracking pipelines. *Nat. Methods* **19**, 829–832 (2022).

71. Tinevez, J.-Y. *et al.* TrackMate: An open and extensible platform for single-particle tracking. *Methods San Diego Calif* **115**, 80–90 (2017).

72. Liu, H., Lin, D. & Yates, J. R. Multidimensional separations for protein/peptide analysis in the post-genomic era. *BioTechniques* **32**, 898, 900, 902 passim (2002).

73. Washburn, M. P., Wolters, D. & Yates, J. R. Large-scale analysis of the yeast proteome by multidimensional protein identification technology. *Nat. Biotechnol.* **19**, 242–247 (2001).

74. Passarge E. Emil Heitz and the concept of heterochromatin: longitudinal chromosome differentiation was recognized fifty years ago. *Am J Hum Genet*. **31**, 106-115 (1979).

Publishing Agreement

It is the policy of the University to encourage open access and broad distribution of all theses, dissertations, and manuscripts. The Graduate Division will facilitate the distribution of UCSF theses, dissertations, and manuscripts to the UCSF Library for open access and distribution. UCSF will make such theses, dissertations, and manuscripts accessible to the public and will take reasonable steps to preserve these works in perpetuity.

I hereby grant the non-exclusive, perpetual right to The Regents of the University of California to reproduce, publicly display, distribute, preserve, and publish copies of my thesis, dissertation, or manuscript in any form or media, now existing or later derived, including access online for teaching, research, and public service purposes.

DocuSigned by:
Dana Renae Kennedy
F3C0DC80D7C5429...
Author Signature

8/29/2024
Date